Targeting the Ataxia Telangiectasia Mutated-null phenotype in chronic lymphocytic leukemia with pro-oxidants

by Angelo Agathanggelou, Victoria J. Weston, Tracey Perry, Nicholas J. Davies, Anna Skowronska, Daniel T. Payne, John S. Fossey, Ceri E. Oldreive, Wenbin Wei, Guy Pratt, Helen Parry, David Oscier, Steve J. Coles, Paul S. Hole, Richard L. Darley, Michael McMahon, John D. Hayes, Paul Moss, Grant Stewart, A. Malcolm R. Taylor, and Tatjana Stankovic

Targeting the Ataxia Telangiectasia Mutated-null phenotype in chronic lymphocytic leukemia with pro-oxidants

Angelo Agathanggelou [1*], Victoria J. Weston[1*], Tracey Perry[1], Nicholas J. Davies[1], Anna Skowronska[1], Daniel T. Payne[2], John S. Fossey[2], Ceri E. Oldreive[1], Wenbin Wei[1], Guy Pratt[1,3], Helen Parry[3], David Oscier[4], Steve J. Coles[5], Paul S. Hole[5], Richard L. Darley[5], Michael McMahon[6], John D. Hayes[6], Paul Moss[1], Grant S. Stewart[1], A. Malcolm R. Taylor[1] and Tatjana Stankovic[1]

[1]School of Cancer Sciences, University of Birmingham, Birmingham, UK; [2]School of Chemistry, University of Birmingham, Birmingham, UK; [3]Haematology Department, Birmingham Heartlands Hospital, Birmingham, UK; [4]Haematology Department, Royal Bournemouth Hospital, Dorset, UK; [5]Department of Haematology, Institute of Cancer and Genetics, Cardiff University School of Medicine, Cardiff, UK; [6]Medical Research Institute, University of Dundee, Dundee, United Kingdom.

Running title: ATM-null CLLs are sensitive to pro-oxidants

Key words: Chronic lymphocytic leukemia, ATM, chemoresistant, oxidative stress, NRF2

Corresponding author: Tatjana Stankovic, School of Cancer Sciences, University of Birmingham, B15 2TT, UK

Email: t.stankovic@bham.ac.uk

Tel: +44(0) 121 414 4496

Fax: +44(0) 121 414 4486

Conflict of interest: There are no conflicts of interest to disclose.

[*]These authors contributed equally to this work.

Abstract (198 words)

Inactivation of the Ataxia Telangiectasia Mutated gene in chronic lymphocytic leukemia results in resistance to p53-dependent apoptosis and inferior responses to treatment with DNA damaging agents. Hence, p53-independent strategies are required to target Ataxia Telangiectasia Mutated-deficient chronic lymphocytic leukemia. As Ataxia Telangiectasia Mutated has been implicated in redox homeostasis, we investigated the effect of the Ataxia Telangiectasia Mutated-null chronic lymphocytic leukemia genotype on cellular responses to oxidative stress with a view to therapeutic targeting. We found that in comparison to Ataxia Telangiectasia Mutated-wild type chronic lymphocytic leukemia, pro-oxidant treatment of Ataxia Telangiectasia Mutated-null cells led to reduced binding of NF-E2 p45-related factor-2 to antioxidant response elements and thus decreased expression of target genes. Furthermore, Ataxia Telangiectasia Mutated-null chronic lymphocytic leukemia cells contained lower levels of antioxidants and elevated mitochondrial reactive oxygen species. Consequently, Ataxia Telangiectasia Mutated-null chronic lymphocytic leukemia, but not tumours with 11q deletion or *TP53* mutations, exhibited differentially increased sensitivity to pro-oxidants both *in vitro* and *in vivo*. We found that cell death was mediated by a p53- and caspase-independent mechanism associated with apoptosis inducing factor activity. Together, these data suggest that defective redox-homeostasis represents an attractive therapeutic target for Ataxia Telangiectasia Mutated-null chronic lymphocytic leukemia.

INTRODUCTION

Chronic lymphocytic leukemia (CLL) with defective DNA damage response (DDR) is refractory to conventional chemotherapeutics (1). The loss of DDR occurs through inactivation of *ATM* and *TP53* genes (2). *ATM* mutations appear in 13-16% of CLLs and are distributed across a large coding region encompassing 64 exons (3, 4). The loss of ATM function typically occurs through the combined effect of 11q deletion (monoalleic *ATM* loss) and an *ATM* mutation, biallelic *ATM* mutations, or less frequently due to the presence of a single mutation, capable of exerting dominant-negative effect on the remaining *ATM* allele (3,4). Compared to CLL tumours with 11q deletion only, those with inactivation of both *ATM* alleles exhibit abrogated DNA damage-induced apoptotic responses *in vitro* and rapid clonal expansion *in vivo*, leading to reduced overall and treatment-free survival (1). Furthermore, in the phase III UK CLL4 trial that compared chlorambucil with fludarabine either alone or in combination with cyclophosphamide, CLL patients with biallelic *ATM* inactivation revealed progression free survival inferior to tumours with a single mutation or 11q deletion, which was second only to tumours with loss/mutation of both *TP53* alleles (5). Early cytogenetic studies showed that CLL progression is associated with the emergence of 11q deleted subclones (6). More recent reports of the dynamic nature of clonal progression has led to the understanding that the selective pressure imparted by DNA damaging agents favours the expansion of pre-existing subclones with defective DDR and consequently successive rounds of treatment with these agents are less effective (7, 8). There is, therefore, a need for therapeutic strategies that act independently of the DDR pathway that can target ATM-null CLL cells.

ATM is a serine/threonine protein kinase activated by DNA double strand breaks (DSBs) that coordinates the activation of cell cycle checkpoints, DNA repair and p53-dependent apoptosis (9). ATM phosphorylates numerous substrates and is involved in the regulation of

a wide range of cellular processes. Consequently, deficiencies in any of these processes caused by the loss of ATM could be used as therapeutic targets (10, 11). Consistent with this notion, ATM-null CLL cells are defective in homologous recombination repair (HRR), a deficiency that can be exploited to induce tumour-specific killing *via* enhanced requirement for HRR upon PARP-inhibition (11).

ATM is also implicated in redox homeostasis (12). Deregulation of redox homeostasis results in oxidative stress and occurs either due to increased reactive oxygen species (ROS) production or reduced antioxidant capacity. A principle antioxidant pathway is regulated by the redox sensitive transcription factor, NF-E2 p45-related factor-2 (NRF2/NFE2L2). In unstressed cells, low levels of NRF2 are maintained through interaction with Kelch-like ECH-associated protein 1 (KEAP1), an adapter for the E3 ubiquitin ligase Cullin 3 (CUL3) that directs NRF2 for proteasomal degradation (13). Modification of redox and electrophile sensitive cysteine residues inhibits the substrate adaptor activity of KEAP1 allowing NRF2 accumulation. The interaction of KEAP1 with NRF2 is further modulated by phosphorylation of NRF2 at serine 40 by protein kinase C (PKC) (14). Within the nucleus, NRF2 forms heterodimers with v-maf musculoaponeurotic fibrosarcoma oncogene homolog (MAF) proteins (MAF-F, G and K) and binds to antioxidant response elements (AREs) in the promoters of target genes such as those required for glutathione synthesis and its own promoter (15). This activity is regulated by the transcriptional repressor BTB and CNC homology 1 transcription factor (BACH1) which competes for the MAF binding partners and for binding to gene promoters (16). In addition, genetic models suggest that binding of Nrf-2 and its activity are regulated by the ATM substrate, Brca1(17).

The most compelling evidence for the role of ATM in redox homeostasis comes from studies of the human radiosensitivity syndrome, Ataxia Telangiectasia (AT), where both *ATM* alleles are inactivated. Cells from these patients display increased oxidative stress as a consequence of elevated levels of ROS, increased oxidised/reduced glutathione (GSSG/GSH) ratio, diminished capacity to scavenge ROS and mitochondrial dysfunction (12, 18). Furthermore, ATM is directly activated by oxidative stress (19) and can exert antioxidant activity through regulation of the pentose-phosphate pathway (20). Recent evidence suggests that ATM might regulate oxidative stress through NRF2. Namely, Nrf2 target gene expression was decreased in Atm-/- murine osteoblasts and this was rescued by the ectopic expression of PKC delta (PKCδ) (21).

In this study, we tested the hypothesis that ATM-null CLLs have an intrinsic defect in their antioxidant defenses which might be exploited to induce synthetic lethality of tumour cells by escalating oxidative stress. We show that compared to ATM-wild type (wt) CLL, ATM-null CLL tumours exhibited defective NRF2-dependent antioxidant transcriptional responses, decreased antioxidant capacity, elevated mitochondrial ROS and increased sensitivity to pro-oxidants both *in vitro* and *in vivo*. Furthermore, we demonstrate that pro-oxidant treatment bypassed the need for a functional DRR and induced cell death *via* a p53- and caspase-independent mechanism involving AIF.

METHODS

Patient samples and cell lines

CLL samples were obtained from Birmingham and Bournemouth Hospitals (Supplementary Table S1). These comprised of 3 CLLs with monoallelic *ATM* loss, 1 monoallelic *ATM* mutant, 3 biallelic *ATM* mutants, 5 with combined *ATM* mutation/deletion and 3 CLLs with

TP53 mutations. All patient samples contained >90% tumour cells. South Birmingham Ethics Committee granted approval for the study. CII, HG3 and PGA isogenic CLL cell lines expressing short hairpin (sh)-RNA against *GFP* or *ATM* were generated as previously described (11).

Chemicals

H_2O_2, *tert*-butylhydroquinone (tBHQ), *N*-acetyl-*p*-benzoquinone imine (NAPQI) and N-phenylmaleimide (Sigma-Aldrich, MO, USA). KU-55933 (Merck KGaA, Darmstadt, Germany), Z-VAD-FMK (EnzoLife Sciences, Exeter, UK). Parthenolide, dimethylamino parthenolide (DMAPT) and DMAPT-hydrochloride (DMAPT-HCl) were isolated and prepared as described (Supplementary Methods, Supplementary Table S2, Supplementary Figure S1, S2, and S3).

Quantitative RT-PCR (Q-PCR)

SYBR-Green quantitative Real-time PCR (Life Technologies) was applied with primers against *NRF2*, *NQO1*, *GCLM*, *GSR* and *HMOX1* (Supplementary Methods). Primers against *β-ACTIN* were used for normalisation and quantification was achieved using the comparative Ct method (22).

XChIP

XChIP was applied to primary CLL samples before and after treatment with 100μM tBHQ for 6 hours using anti-NRF2 and pre-immune antisera as previously described (23, and Supplementary Methods).

Biochemical assays

GSH was quantified using a Glutathione Assay Kit (Sigma-Aldrich). To determine GSSG, GSH was first derivatised with N-ethylmaleimide (Sigma-Aldrich). Levels of NADPH and NADP$^+$ were quantified using an NADP/NADPH assay kit (Abcam, Cambridge, UK).

Mitochondrial ROS Assay

Mitochondrial superoxide was detected using MitoSox Red (Life Technologies) in accordance with the manufacturer's instructions and quantified using a LSR II flow cytometer (BD Biosciences, Oxford, UK) (Supplementary Methods).

RNA knockdown

Knockdown of gene expression in HaCat cells was achieved by transfection of siRNAs against ATM, KEAP1, BRCA1 or Scrambled siRNA with Oligofectamine (Life Technologies) in accordance with the manufacturer's instructions (Supplementary Methods, Supplementary Table S4).

Immunoblotting

Immunoblotting was performed as previously described (24, Supplementary Methods).

Murine xenograft

Animals were treated in accordance with United Kingdom Home Office guidelines, Schedule 1. Subcutaneous tumours were initiated by injection of 5×10^6 CII-isogenic cell lines with and without stable ATM-knockdown into six week old NOD.Cg-$Prkdc^{scid}$ $Il2rg^{tm1Wjl}$/SzJ (NSG) mice. Tumours were grown for 15 days prior to treatment with 6 mg/kg parthenolide or vehicle *via* intra-peritoneal injection for 5 days.

Primary CLL tumour cells were engrafted as previously described (25). Briefly, 6-week old NSG mice were sublethally irradiated (1.25Gy) prior to intravenous co-injection of 50×10^6 PBMC from an ATM-null CLL patient and 10×10^3 CD14$^+$ monocytes from a healthy donor. After three days, mice were randomised and treated with a daily dose of either 100mg/kg DMAPT-HCl or vehicle by oral gavage for 9 days. Splenic tumour burden was assessed by FACS analysis.

Statistics

In vitro and *in vivo* data were analysed using *paired* or *unpaired* 2-tailed Student's *t*-tests. Data are presented as ± standard error of the mean (SEM).

RESULTS

Defective NRF2-regulated gene expression in ATM-null CLL cells

We have investigated the effect of ATM loss on NRF2 directed antioxidant responses by treating a panel of CLL tumours with H_2O_2 and measuring the induction of gene expression by Q-PCR. H_2O_2 induced a 1.7-3.0 fold increase in NRF2 target gene expression in ATM-wt tumours (n=4), whereas induction was significantly impaired in ATM-null CLLs (n=4) (Figure 1A). Examination of previously generated expression data supported this observation (26). Following exposure to IR, an insult that generates ROS, up-regulation of 40 NRF2 regulated

transcripts was significantly (p<0.05) impaired in ATM-null CLLs (n=6) compared to ATM-wt CLLs (n=5) (Supplementary Figure S4A).

To investigate a possible role for KEAP1 in the defective induction of NRF2 target genes in ATM-null CLL, KEAP1 activity was inhibited pharmacologically or by siRNA knockdown. Tumour cells were treated with tBHQ, the quinone radical of which is an electrophile that covalently modifies cysteine residues in KEAP1 preventing it from targeting NRF2 for degradation. In ATM-wt tumours (n=5), high dose tBHQ (100 µM) induced a 5-71 fold up-regulation of NRF2 target genes (Figure 1B). In comparison, significantly lower expression (0.5-4.3 fold) was induced in ATM-null tumours (n=5). A similar differential was observed with low dose tBHQ (10 µM) indicating that the defective expression in ATM-null CLLs was not due to toxicity (Supplementary Figure S4B).

In accordance with a previous report, knockdown of KEAP1 also induced the expression of NRF2 target genes (27). Inhibition of ATM function by siRNA-knockdown (n=3) (Figure 1C) or ATM-inhibitor (n=3) (Figure 1D) abolished induction of NRF2-target genes. These data indicated that the defective regulation of NRF2 transcripts in ATM deficient cells occurs downstream of KEAP1 function.

Consistent with an absence of a defect in the regulation of NRF2 by KEAP1 the expression of NRF2 mRNA and protein was comparable in ATM-wt and ATM-null tumors (Supplementary Figure S4C, S4D). Following treatment with tBHQ, no difference was observed between ATM-wt and ATM-null CLLs regarding the change in levels of NRF2 or other proteins involved in this antioxidant pathway: KEAP1, BACH1 and MAF protein (Supplementary Figure S4D, S4E, S4F).

A previous study suggested that ATM regulates NRF2 through PKCδ (21). However, in keeping with the data from a proteomic study of ATM substrates (10), we found no interaction between ATM and NRF2 in co-immunoprecipitation assay (Supplementary Figure S5A). Furthermore, we did not detect an interaction between ATM and PKCδ and loss of ATM did not alter the levels of PKCδ or the levels of phosphorylated-serine on NRF2 (Supplementary Figure S5B and S5C).

Brca1 was previously found to regulate Nrf-2 transcriptional activity (17). Therefore, we next investigated the possibility that ATM co-operates with BRCA1 in the regulation of NRF2 activity. We found reduced induction of antioxidant genes in cells treated with either ATM or BRCA1-specific siRNAs (Figure 1F and 1G). This defect was not increased by the combined knockdown of both genes suggesting ATM and BRCA1 may act in the same pathway that regulates NRF2 function.

These data suggest that in CLL cells, loss of ATM-function induces a defect in NRF2 regulated gene expression that is independent of PKCδ, KEAP1, BACH1 and MAF proteins and may involve co-operation with BRCA1.

ATM-loss reduces binding of NRF2 to antioxidant response elements

In the absence of any defect in the regulation of NRF2 protein levels we considered whether the transcriptional deregulation in ATM-null CLL tumours arises at the point of NRF2 binding to AREs. We used XChIP and Q-PCR to measure tBHQ-induced binding of NRF2 to an ARE in the promoter region of the prototypic NRF2 target gene *NQO1*. Consistent with the

observed difference in gene induction, significantly less NRF2 bound to the promoter region of *NQO1* in ATM-null CLL compared to wild-type tumours (Figure 1E). This suggests that the reduced NRF2 dependent transcription in ATM-null primary CLL cells is caused by defective binding of NRF2 to AREs.

ATM-null CLL cells exhibit reduced antioxidant capacity, elevated mitochondrial superoxide and increased sensitivity to pro-oxidants

In agreement with the effect on antioxidant transcriptional responses, the level of total cellular glutathione was significantly lower in ATM-null compared to ATM-wt primary CLL (Figure 2A). This effect was recapitulated in three isogenic CLL cell lines with stable knockdown of ATM (Supplementary Figure S6A).

The regeneration of GSH from GSSG is catalysed by glutathione reductase (GSR) utilising NADPH as a cofactor. In ATM-wt tumours, virtually all glutathione was in the reduced form (GSH) whereas in ATM-null tumours only 70% was reduced and 30% was oxidised (GSSG), indicating increased oxidative stress in these cells (Figure 2B). Accordingly, the pool of NADP$^+$ was significantly elevated in ATM-null compared to ATM-wt CLLs (Figure 2C).

A-T cells display continuous oxidative stress due to intrinsic mitochondrial dysfunction and contain elevated superoxide levels (28). To determine whether ATM-null CLL cells share this phenotype, the levels of mitochondrial ROS were examined using the mitochondrial superoxide sensitive dye, MitoSox Red. Consistent with observations in A-T cells, mitochondrial ROS levels were significantly higher in ATM-null (n=3) than wild-type CLLs (n=3) (p=0.007) (Figure 2D, 2E).

Increased mitochondrial ROS damages the organelle promoting further dysfunction in a positive-feedback loop (28). To test whether this occurs in ATM-null CLLs, tumours were exposed to extracellular ROS. H_2O_2 induced significantly higher levels of mitochondrial superoxide in ATM-null CLLs (n=3) compared to wild-type CLLs (n=3) at all concentrations tested (Figure 2E). This suggests that the intrinsic mitochondrial dysfunction associated with ATM-deficiency can be further exacerbated using exogenous sources of ROS. Examination of mitochondrial DNA content showed that both ATM-null and ATM-wt CLL contained a comparable number of mitochondria but significantly more than PBMCs from normal donors (Supplementary Figure S6B) indicating that the increased mitochondrial ROS in ATM-null CLL is the result of mitochondrial dysfunction rather than mitochondrial number.

This data suggests that ATM-null CLL cells are under greater oxidative stress than their wild-type counterparts.

ATM-null CLL cells show increased sensitivity to pro-oxidants *in vitro* and *in vivo*

In view of the increased oxidative stress in ATM-null CLL cells, we determined if this translated to increased sensitivity to pro-oxidant treatment. ATM-null CLLs (n=6) were significantly more sensitive to H_2O_2 than ATM-wt CLLs (n=9) *in vitro* (Figure 2F). The effect of ATM-deficiency on H_2O_2 sensitivity was confirmed in a CII-isogenic cell line with stable knockdown of ATM (Supplementary Figure S7A).

Next, we addressed the sensitivity of ATM-null and wild-type primary CLLs to NAPQI and parthenolide, pro-oxidants that induce oxidative stress by depleting glutathione (GSH) (29, 30). ATM-null tumours were significantly more sensitive than wild-type to both reagents

(Figure 2G, 2H). The effects of H_2O_2, NAPQI and parthenolide were associated with oxidative damage, as treatment with N-acetyl cysteine (NAC), a glutathione precursor, protected cells (Supplementary Figure S7B, S7C, S7D). Importantly, the tumour specific activity of both H_2O_2 and parthenolide was confirmed using PBMCs from normal donors (Supplementary Figure S7E, S7F).

To determine if the increased sensitivity to pro-oxidants was specific to the ATM-null status we examined primary CLL cells with monoallelic 11q deletion or *TP53* mutations. The sensitivity of CLLs with either genotype did not significantly deviate from wild-type CLLs suggesting that increased sensitivity to pro-oxidants is specifically associated with the ATM functional loss (Supplementary Figure S7G, S7H).

The *in vivo* efficacy of pro-oxidant therapy on ATM-deficient CLL was examined using two murine xenograft models. First, a subcutaneous xenograft model of CII-isogenic cell lines with and without stable ATM-knockdown was established. Parthenolide significantly inhibited the growth of ATM-knockdown tumours compared to either vehicle treated cells or to parthenolide treated wild type tumours (44.0% vs 9.7%), Figure 3A.

Finally, an ATM-null primary CLL xenograft was established and for or systemic pro-oxidant treatment, dimethylamino parthenolide-hydrochloride (DMAPT-HCl), a water-soluble and orally bioavailable form of parthenolide (31), was generated. Quantification of engrafted splenic CLL cells demonstrated that pro-oxidant therapy significantly reduced hCD19^{+} tumour cell burden ($p<0.05$) (Figure 3B). Furthermore, engrafted cells displayed increased levels of 8-oxo-dG, indicating oxidative stress was induced following pro-oxidant treatment (Figure 3C).

This data shows that pro-oxidant based therapies are effective against chemoresistant ATM-null CLL tumours *in vitro* and *in vivo*.

Pro-oxidant induced cell death in CLL is p53/caspase-independent and involves AIF

Since the DDR is defective in ATM-null CLL, a DDR-independent pathway must be operating to facilitate pro-oxidant induced cell death. Consistent with this, activation of the DDR was not detected in either ATM-null or wild-type CLL cells following treatment with therapeutically effective concentrations of H_2O_2 (Supplementary Figure S8), NAPQI or parthenolide (data not shown). To elucidate the mechanism of cell death induced by pro-oxidants, ATM-null primary CLL tumours were treated with NAPQI or H_2O_2 with and without pan-caspase inhibitor. Caspase inhibition did not significantly affect NAPQI or H_2O_2-induced cell death of ATM-null primary CLL tumours (Figure 4A, 4B). This was confirmed by immunoblotting in CII-isogenic cell lines which showed that in contrast to ionising radiation, PARP1-cleavage was not induced by NAPQI (Figure 4C).

Next, we investigated the induction of cell death by an alternative mechanism involving the cellular redistribution of apoptosis inducing factor (AIF). In response to stress, AIF is released from the mitochondria as a cleaved 57kDa pro-apoptotic protein (tAIF) which translocates to the nucleus where it cooperates with endonuclease G to cause large scale DNA fragmentation and chromatin condensation (32). In untreated cells, AIF staining colocalised with mitochondria (Figure 4D), whereas treatment with H_2O_2 led to nuclear translocation (Figure 4E, 4F). In agreement with the differential sensitivity of ATM-null CLL tumours to pro-oxidants, nuclear tAIF was induced with 10 μM H_2O_2 whereas in ATM-wt CLLs, 40 μM H_2O_2 was required to elicit the same effect (Figure 4F). Inhibition of AIF

prevented H_2O_2-induced digestion of genomic DNA into ~50kb fragments, thus confirming the role of AIF in this process (Figure 4G).

These data demonstrate that pro-oxidants induce p53 and caspase-independent cell death in wild-type and ATM-null CLL associated with nuclear translocation of AIF.

DISCUSSION

We show that the ATM-null phenotype in CLL can be targeted with pro-oxidant based therapies to induce selective killing. We demonstrate that a defect in the NRF2-directed antioxidant response is present in ATM-null primary CLLs. This correlated with reduced antioxidant capacity, increased mitochondrial ROS and increased sensitivity to pro-oxidants *in vitro* and *in vivo*. Previous reports have demonstrated increased sensitivity of CLL cells to pro-oxidant based therapies compared to non-tumour cells, but this is the first study to demonstrate that this approach specifically targets the ATM-null phenotype in CLL (33, 34).

Our data suggest that binding of NRF2 to target gene AREs is reduced in ATM-null CLL despite normal levels of NRF2, KEAP1, BACH1 and MAF proteins and normal levels of NRF2/MAF heterodimerisation. Previous studies indicated that reduced PKCδ levels might contribute to defective Nrf-2 regulation in Atm-/- mice and that NRF2 stability is regulated by phosphorylation at ser40 by PKC (14, 21). We observed that PKCδ and serine-phosphorylated NRF2 levels are unaffected by the loss of ATM in CLL cells and that in agreement with previous proteomic screen (10), both PKCδ and NRF2 are unlikely to be ATM substrates. In search for the mechanism of reduced NRF2 activity in ATM null cells we confirmed the role of BRCA1 in the regulation of the NRF2 antioxidant response.

15

Furthermore, by showing that the combined knockdown of ATM and BRCA1 does not cause further deregulation we demonstrate that ATM and BRCA1 function in the same pathway to regulate NRF2-antioxidant responses.

Previously, we have reported that ATM-null tumours are refractory to conventional DNA damaging therapies due to inactivation of the p53-dependent apoptosis pathway (1, 35), underscoring the need for a p53-independent strategy for the treatment of these tumours. In this study, we found that ATM-null cells are differentially sensitive to pro-oxidants as reflected by the appearance of tAIF in the nuclei of these cells at lower concentrations of H_2O_2 than in ATM-wt cells. The higher level of mitochondrial superoxide in ATM-null CLLs indicated mitochondrial dysfunction. Pro-oxidant treatment is likely to further damage the mitochondria, thus triggering the translocation of AIF and p53-independent cell death. Recent studies also suggest AIF translocation may occur due to an increase in inducible nitric oxide synthase (iNOS) activity following stimulation of JNK by ROS and the subsequent activation of ERK1/2 (36). In addition, ROS can induce the caspase-independent activation of the BH3 interacting domain death agonist (BID), thus leading to AIF translocation (37).

Most importantly, using a pro-oxidant based strategy we show that ATM-null CLL cells are significantly more sensitive than ATM-wt tumours and non-tumour cells to agents previously shown to stimulate NRF2-mediated adaptation to stress (38, 39). Thus both NAPQI and parthenolide represent novel clinically applicable approaches for the treatment of ATM-null CLL. Of note, acetaminophen, the NAPQI precursor, has previously been used in a phase I trial for the treatment of metastatic melanoma (40) as an approach to enhance the specificity of anti-cancer agents which deplete glutathione. Similarly, parthenolide and its water soluble

derivative, DMAPT, have been shown to have activity against hematopoietic malignancies, including chemo-refractory CLL and acute myeloid leukemia (41, 42).

Targeting oxidative stress to bypass the defect in p53-dependent apoptosis is an attractive therapeutic strategy for several reasons. First, genetic variations present a challenging problem with respect to the treatment of CLL (8, 43) and elevated oxidative stress can impact on disease progression by inducing oxidative DNA damage (44) and increasing the mutation rate that supports clonal diversity. Indeed, in CLL, oxidative stress is present early in the genesis of disease and is detectable at the stage of pre-malignant monoclonal B-lymphocytosis (45). Thus to avoid the selection of adverse subclones with ATM-deficiency that occurs with conventional genotoxic agents (7, 8), it is preferable to target stress phenotypes common to all tumour cells and, as in this case, potential mechanisms of diversification (46). Furthermore, elevated oxidative stress may provide a selective advantage for ATM-null CLL cells regarding their interactions with immune cells within lymphoid tissues. The activity of surrounding immune cells is suppressed by ROS and therefore, loss of ATM and the associated increase in ROS production may facilitate immune evasion (47). Finally, loss of ATM and the associated decrease in antioxidant levels may render the tumour cells more dependent on stromal cells for redox support (48), thus providing a rationale for combined therapeutic approaches with pro-oxidants and inhibitors of tumour/microenvironment interactions.

Recently a number of p53-indendent treatments for CLL became available. These include use of immunomodulatory agents as well as inhibitors of B cell receptor signalling that target either Bruton Tyrosine Kinase (Ibrutininb) or PI3 kinase delta (Idelalisib) (49). Pro-oxidant based therapies utilise oxidative stress as a cellular weakness of leukemic cells and

represent an example of a synthetic lethality approach. It will be of interest to determine whether pro-oxidants could be used in combination with new targeted treatments to increase the benefit for patients with the ATM-null CLL phenotype.

Finally, it is important to note that the roles in DDR and oxidative stress responses denote two separate ATM functions. ATM is activated by oxidation of the cysteine residue at position 2991 in the FATC domain leading to formation of disulphide cross-linked dimers (19). ATM mutated at C2991 is unresponsive to oxidative stress despite normal response to DNA damage. This raises the possibility that certain *ATM* mutations may not affect DDR and still render a phenotype amenable for targeting by pro- oxidants.

In summary, we show that the oxidative stress phenotype is a valid therapeutic target in the treatment of ATM-null CLL due to the intrinsic deficiencies in redox homeostasis. Significantly, this mode of therapy bypasses the DDR defect found in ATM-null CLL cells and therefore represents a feasible approach for treatment of patients that harbor these subclones.

Authorship

Contribution: AA and VJW designed, performed experiments, interpreted data and wrote manuscript; TP, ND and AS performed experiments; DTP and JSF extracted parthenolide, synthesised DMAPT and data analysis thereof, co-wrote portions of the manuscript and supplementary material; CEO and WW performed analysis; GP, HP, DO, RLD and JDH designed the work and wrote the manuscript; SJC, PSH, MM, GSS analysed data; AMRT, PM, TS designed the work, interpreted data and wrote the manuscript.

References:

1.   Austen B, Skowronska A, Baker C, et al. Mutation status of the residual ATM allele is an important determinant of the cellular response to chemotherapy and survival in patients with chronic lymphocytic leukemia containing an 11q deletion. J Clin Oncol. 2007;25(34):5448-5457.

2.   Trbusek M, Malcikova J. TP53 aberrations in chronic lymphocytic leukemia. Adv Exp Med Biol. 2013;792:109-31.

3.   Austen B, Powell JE, Alvi A, et al. Mutations in the ATM gene lead to impaired overall and treatment-free survival that is independent of IGVH mutation status in patients with B-CLL. Blood. 2005;106(9):3175-3182.

4.   Navrkalova V, Sebejova L, Zemanova J, et al. ATM mutations uniformly lead to ATM dysfunction in chronic lymphocytic leukemia: application of functional test using doxorubicin. Haematologica. 2013;98(7):1124-1131.

5.   Skowronska A, Parker A, Ahmed G, et al. Biallelic ATM inactivation significantly reduces survival in patients treated on the United Kingdom Leukemia Research Fund Chronic Lymphocytic Leukemia 4 trial. J Clin Oncol. 2012;30(36):4524-4532.

6.   Fegan C, Robinson H, Thompson P, Whittaker JA, White D. Karyotypic evolution in CLL: identification of a new sub-group of patients with deletions of 11q and advanced or progressive disease. Leukemia. 1995;9(12):2003-2008.

7.   Ouillette P, Saiya-Cork K, Seymour E, Li C, Shedden K, Malek SN. Clonal evolution, genomic drivers, and effects of therapy in chronic lymphocytic leukemia. Clin Cancer Res. 2013;19(11):2893-2904.

8.   Landau DA, Carter SL, Stojanov P, et al. Evolution and impact of subclonal mutations in chronic lymphocytic leukemia. Cell. 2013;152(4):714-726.

9.   Lavin MF. Ataxia-telangiectasia: from a rare disorder to a paradigm for cell signalling and cancer. Nat Rev Mol Cell Biol. 2008;9(10):759-769.

10.   Matsuoka S, Ballif BA, Smogorzewska A, et al. ATM and ATR substrate analysis reveals extensive protein networks responsive to DNA damage. Science. 2007;316(5828):1160-1166.

11.   Weston VJ, Oldreive CE, Skowronska A, et al. The PARP inhibitor olaparib induces significant killing of ATM-deficient lymphoid tumor cells in vitro and in vivo. Blood. 2010;116(22):4578-4587.

12.   Ambrose M, Gatti RA. Pathogenesis of ataxia-telangiectasia: the next generation of ATM functions. Blood. 2013;121(20):4036-4045.

13.   Kobayashi A, Kang MI, Okawa H, et al. Oxidative stress sensor Keap1 functions as an adaptor for Cul3-based E3 ligase to regulate proteasomal degradation of Nrf2. Mol Cell Biol. 2004;24(16):7130-7139.

14.   Huang HC, Nguyen T, Pickett CB. Phosphorylation of Nrf2 at Ser-40 by protein kinase C regulates antioxidant response element-mediated transcription. J Biol Chem. 2002;277(45):42769-42774.

15.   Itoh K, Chiba T, Takahashi S, et al. An Nrf2/small Maf heterodimer mediates the induction of phase II detoxifying enzyme genes through antioxidant response elements. Biochem Biophys Res Commun. 1997;236(2):313-322.

16.   Dhakshinamoorthy S, Jain AK, Bloom DA, Jaiswal AK. Bach1 competes with Nrf2 leading to negative regulation of the antioxidant response element (ARE)-mediated NAD(P)H:quinone oxidoreductase 1 gene expression and induction in response to antioxidants. J Biol Chem. 2005;280(17):16891-16900.

17.   Gorrini C, Baniasadi PS, Harris IS, et al. BRCA1 interacts with Nrf2 to regulate antioxidant signaling and cell survival. J Exp Med. 2013;210(8):1529-1544.

18.   Valentin-Vega YA, Maclean KH, Tait-Mulder J, et al. Mitochondrial dysfunction in ataxia-telangiectasia. Blood. 2012;119(6):1490-1500.

19.   Guo Z, Kozlov S, Lavin MF, Person MD, Paull TT. ATM activation by oxidative stress. Science. 2010;330(6003):517-521.

20. Cosentino C, Grieco D, Costanzo V. ATM activates the pentose phosphate pathway promoting anti-oxidant defence and DNA repair. EMBO J. 2011;30(3):546-55.

21. Li B, Wang X, Rasheed N, et al. Distinct roles of c-Abl and Atm in oxidative stress response are mediated by protein kinase C delta. Genes Dev. 2004;18(15):1824-1837.

22. Schmittgen TD, Livak KJ. Analyzing real-time PCR data by the comparative C(T) method. Nat Protoc. 2008;3(6):1101-1108.

23. Nowak DE, Tian B, Brasier AR. Two-step cross-linking method for identification of NF-kappaB gene network by chromatin immunoprecipitation. Biotechniques. 2005;39(5):715-725.

24. Stankovic T, Weber P, Stewart G, et al. Inactivation of ataxia telangiectasia mutated gene in B-cell chronic lymphocytic leukaemia. Lancet. 1999;353(9146):26-29.

25. Bagnara D, Kaufman MS, Calissano C, et al. A novel adoptive transfer model of chronic lymphocytic leukemia suggests a key role for T lymphocytes in the disease. Blood. 2011;117(20):5463-5472.

26. Stankovic T, Hubank M, Cronin D, et al. Microarray analysis reveals that TP53- and ATM-mutant B-CLLs share a defect in activating proapoptotic responses after DNA damage but are distinguished by major differences in activating prosurvival responses. Blood. 2004;103(1):291-300.

27. Devling TW, Lindsay CD, McLellan LI, McMahon M, Hayes JD. Utility of siRNA against Keap1 as a strategy to stimulate a cancer chemopreventive phenotype. Proc Natl Acad Sci U S A. 2005;102(20):7280-7285A.

28. Quick KL, Dugan LL. Superoxide stress identifies neurons at risk in a model of ataxia-telangiectasia. Ann Neurol. 2001;49(5):627-635.

29. Hinson JA. Reactive metabolites of phenacetin and acetaminophen: a review. Environ Health Perspect. 1983;49:71-79.

30. Skalska J, Brookes PS, Nadtochiy SM, et al. Modulation of cell surface protein free thiols: a potential novel mechanism of action of the sesquiterpene lactone parthenolide. PLoS One. 2009;4(12):e8115.

31. Neelakantan S, Nasim S, Guzman ML, Jordan CT, Crooks PA. Aminoparthenolides as novel anti-leukemic agents: Discovery of the NF-kappaB inhibitor, DMAPT (LC-1). Bioorg Med Chem Lett. 2009;19(15):4346-4349.

32. Susin SA, Lorenzo HK, Zamzami N, Marzo I, Snow BE, Brothers GM, et al. Molecular characterization of mitochondrial apoptosis-inducing factor. Nature. 1999;397(6718):441-446.

33.   Farber CM, Liebes LF, Kanganis DN, Silber R. Human B lymphocytes show greater susceptibility to H2O2 toxicity than T lymphocytes. J Immunol. 1984;132(5):2543-2546.

34.   Wu RP, Hayashi T, Cottam HB, et al. Nrf2 responses and the therapeutic selectivity of electrophilic compounds in chronic lymphocytic leukemia. Proc Natl Acad Sci U S A. 2010;107(16):7479-7484.

35.   Pettitt AR, Sherrington PD, Stewart G, Cawley JC, Taylor AM, Stankovic T. p53 dysfunction in B-cell chronic lymphocytic leukemia: inactivation of ATM as an alternative to TP53 mutation. Blood. 2001;98(3):814-822.

36.   Chowdhury AA, Chaudhuri J, Biswas N, et al. Synergistic apoptosis of CML cells by buthionine sulfoximine and hydroxychavicol correlates with activation of AIF and GSH-ROS-JNK-ERK-iNOS pathway. PLoS One. 2013;8(9):e73672.

37.   Tobaben S, Grohm J, Seiler A, Conrad M, Plesnila N, Culmsee C. Bid-mediated mitochondrial damage is a key mechanism in glutamate-induced oxidative stress and AIF-dependent cell death in immortalized HT-22 hippocampal neurons. Cell Death and Differentiation. 2011;18(2):282-292.

38.   Jeong WS, Keum YS, Chen C, et al. Differential expression and stability of endogenous nuclear factor E2-related factor 2 (Nrf2) by natural chemopreventive compounds in HepG2 human hepatoma cells. J Biochem Mol Biol. 2005;38(2):167-176.

39.   Copple IM, Goldring CE, Jenkins RE, Hayes JD, et al. The hepatotoxic metabolite of acetaminophen directly activates the Keap1-Nrf2 cell defense system. Hepatology. 2008;48(4):1292-1301.

40.   Wolchok JD, Williams L, Pinto JT, et al. Phase I trial of high dose paracetamol and carmustine in patients with metastatic melanoma. Melanoma Res. 2003;13(2):189-196.

41.   Guzman ML, Rossi RM, Neelakantan S, et al. An orally bioavailable parthenolide analog selectively eradicates acute myelogenous leukemia stem and progenitor cells. Blood. 2007;110(13):4427-4435.

42.   Steele AJ, Jones DT, Ganeshaguru K, et al. The sesquiterpene lactone parthenolide induces selective apoptosis of B-chronic lymphocytic leukemia cells in vitro. Leukemia. 2006;20(6):1073-1079.

43.   Landau DA, Carter SL, Getz G, Wu CJ. Clonal evolution in hematological malignancies and therapeutic implications. Leukemia. 2013;28(1):34-43.

44.   Oltra AM, Carbonell F, Tormos C, Iradi A, Saez GT. Antioxidant enzyme activities and the production of MDA and 8-oxo-dG in chronic lymphocytic leukemia. Free Radic Biol Med. 2001;30(11):1286-1292.

45.   Collado R, Oliver I, Tormos C, et al. Early ROS-mediated DNA damage and oxidative stress biomarkers in Monoclonal B Lymphocytosis. Cancer Lett. 2012;317(2):144-149.

46.   Luo J, Solimini NL, Elledge SJ. Principles of cancer therapy: oncogene and non-oncogene addiction. Cell. 2009;136(5):823-837.

47.   Jitschin R, Hofmann AD, Bruns H, et al. Mitochondrial metabolism contributes to oxidative stress and reveals therapeutic targets in chronic lymphocytic leukemia. Blood. 2014;123(17):2663-2672.

48.   Zhang W, Trachootham D, Liu J, et al. Stromal control of cystine metabolism promotes cancer cell survival in chronic lymphocytic leukaemia. Nat Cell Biol. 2012;14(3):276-286.

49.   Byrd JC, Jones JJ, Woyach JA, Johnson AJ, Flynn JM. Entering the Era of Targeted Therapy for Chronic Lymphocytic Leukemia: Impact on the Practicing Clinician. J Clin Oncol. 2014;32(27):3039-3047.

50.   Blocher D. n CHEF I electrophoresis a linear induction of dsb corresponds to a nonlinear fraction of extracted DNA with dose. Int J Radiat Biol. 1990;57(1):7-12.

FIGURE LEGENDS

Figure 1. Induction of the NRF2 antioxidant response is defective in ATM-null CLL primary tumours. (A) Q-PCR showing differentially reduced induction of transcription of the NRF2-target genes (*NRF2*, *GCLM*, *NQO1*, *HMOX1* and *GSR*) in ATM-wt compared to ATM-null primary CLL samples following 6 hours treatment with 100µM H_2O_2 and (B) 100µM tBHQ. (C) Q-PCR showing reduced induction of the NRF2 target genes in HaCaT cells following KEAP1-knockdown with and without ATM-knockdown (n=3) or (D) incubation of KEAP1- knockdown HaCaT cells with 10µM ATM kinase inhibitor KU-55933 (ATMi) (n=3). The inhibitor was added 48hrs after transfection and incubated for 24hrs. Data were normalised to β-ACTIN and expressed as fold-change relative to untreated cells using the comparative Ct method. (E) XChIP assay showing defective tBHQ-induced binding of NRF2 to *ARE* in the promoter of *NQO1* in ATM-null CLL cells compared to ATM-wt CLLs. XChIP was undertaken in accordance with the protocol described (23). DNA was

immunoprecipitated using anti-NRF2 antibody or Pre-immune control. Enriched DNA was amplified using Q-PCR and data expressed as percentage of input. (F) Q-PCR showing the effect of ATM and BRCA1 knockdowns on tBHQ or (G) H_2O_2 induced expression of NRF2 target gene NQO1 (n=3). Statistical significance was determined using Student's *t*-test, p-values less than 0.05 (*), 0.01 (**), 0.001 (***) were considered significant. Error bars represent SEM.

Figure 2. ATM-null CLL cells exhibit decreased antioxidant content, elevated levels of mitochondrial superoxide and differential sensitivity to pro-oxidant agents

(A) Total glutathione expressed relative to the levels in ATM wild-type cells are reduced in ATM-null primary CLL samples. (B) The ratios of GSSG:GSH and (C) $NADP^+$:NADPH are differentially increased in ATM-null primary CLL tumours. (D) Mitochondrial superoxide measured by flow cytometry is differentially increased in ATM-null CLL tumours treated for 1 hour with 0-25μM H_2O_2. Cells were dual stained with Annexin V-APC to permit exclusion of double-positive cells undergoing apoptosis. A representative dot plot is shown and (E) quantification is presented. ATM-null CLL primary tumours show differential sensitivity following treatment with (F) H_2O_2, (G) NAPQI or (H) parthenolide for 24h. The surviving fraction was determined by flow cytometry (Beckman Coulter MCL-Epics flow cytometer) with Annexin V-FITC/propidium iodide labeling. The statistical significance was determined using Student's *t*-test, p-values less than 0.05 (*), 0.01 (**), 0.001 (***) were considered significant. Error bars represent SEM.

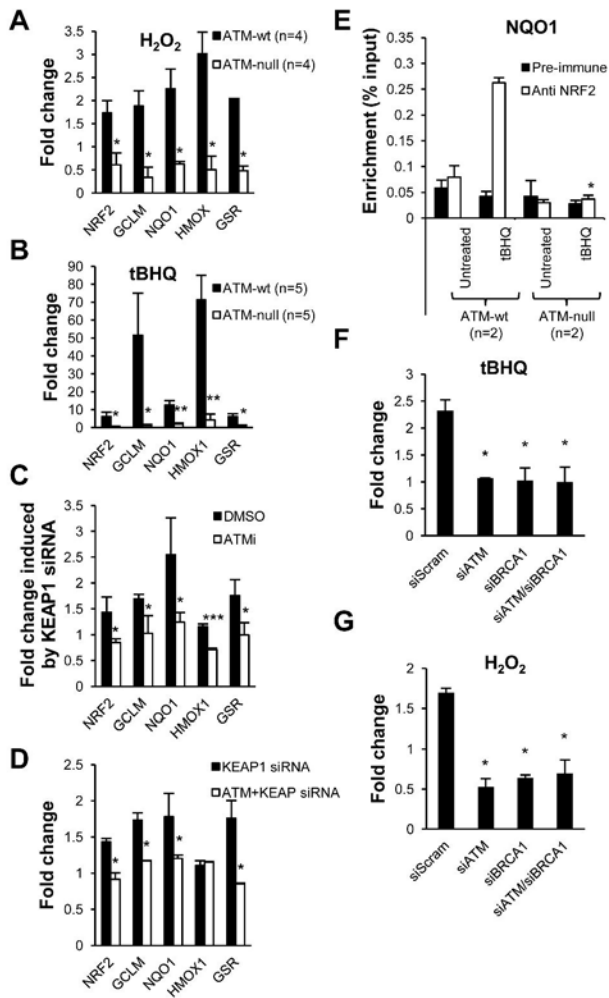**Figure 3. ATM-null cells are targeted by pro-oxidants *in vivo*.**

(A) Subcutaneous xenografts of ATMshRNA (n=7) and GFPshRNA (n=7) expressing CII-isogeneic cell lines were treated with 6mg/kg parthenolide or vehicle by intraperitoneal
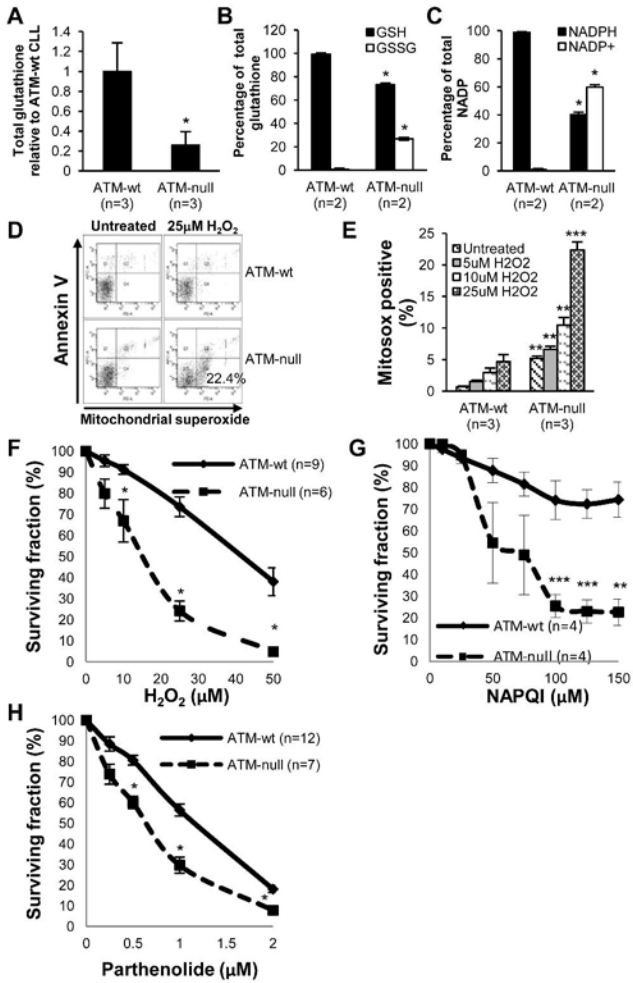
injection for 5 days leading to a significant reduction in tumour volume. Tumour volume was calculated using the formula Vol = 0.5 x L x W^2 before and after treatment. (B) Xenografts of ATM-null primary CLL were established and treated by oral gavage with vehicle (n=5) or 100mg/kg dimethylaminoparthenolide (DMAPT) (n=5) for 9 days, leading to a significant reduced splenic tumour burden in DMAPT-treated animals, as determined by flow cytometry using antibodies against hCD19 (cl.HIB19), hCD3 (cl.SK7), hCD45 (cl.2D1) and mCD45 (cl.30-F11) (eBioscience Inc, San Diego, CA, USA) and CountBright absolute counting beads (Life Technologies). (C) Histological sections depicting differentially increased splenic 8-oxo-dG expression in DMAPT treated xenografts. Brown labeling indicates immobilization of anti-hCD19 (eBioscience) and anti-8-oxo-dG (Abcam) antibodies. Nuclei were counterstained blue with hematoxylin and images were captured at 200x magnification. Statistical significance was determined using Student's *t*-test, p-values less than 0.05 (*) were considered significant. Error bars represent SEM.
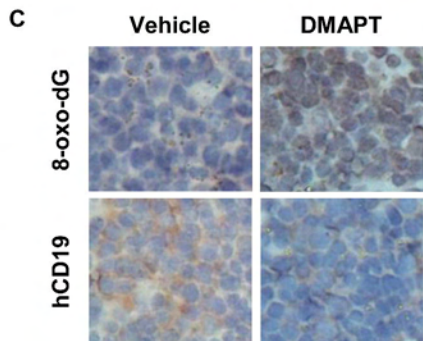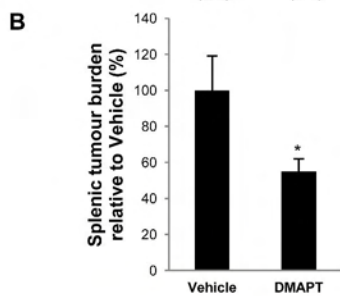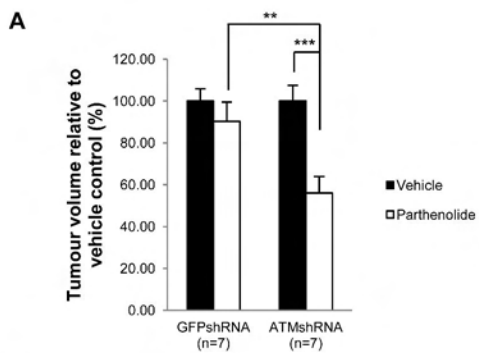
Figure 4. Pro-oxidant treatment induces caspase-independent, AIF-dependent apoptosis.

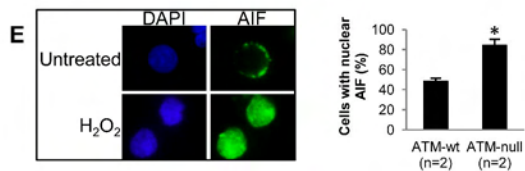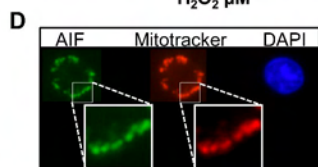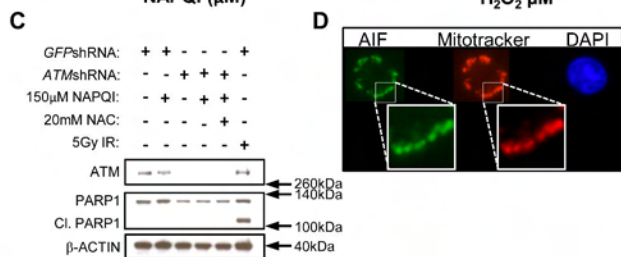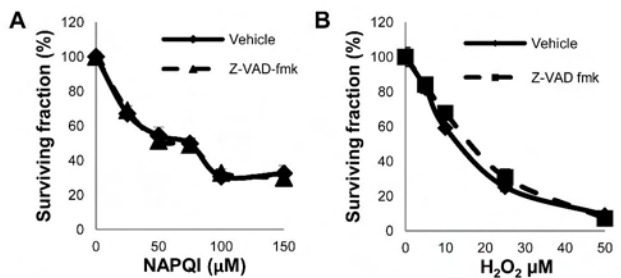Representative ATM-null primary CLL tumours were treated with (A) NAPQI or (B) H_2O_2 for 24h in the presence or absence of 20µM pan-caspase inhibitor (Z-VAD-FMK). The effect on apoptosis was analysed using Annexin-V/PI labelling and flow cytometry. (C) Isogenic CII CLL cell lines were treated with NAPQI with and without antioxidant (NAC) for 24h or irradiated (IR) and PARP cleavage induction visualised by immunoblotting. Anti-ATM (cl.11G12, Abcam), demonstrates ATM-knockdown and anti-ACTIN antibody (Sigma) was used as the loading control. (D) Immunofluorescence labelling shows colocalisation of AIF (rabbit anti-AIF, Santa Cruz) (green) with mitochondria (MitotrackerRed, Life Technologies) (red). Nuclei were counterstained with DAPI (blue). (E) ATM-wt and ATM-null primary CLL cells were treated with 10µM and 40µM H_2O_2 for 6hr and labelled with anti-AIF antibody.

Histogram shows quantification of cells with nuclear AIF. (F) Immunoblot of cellular fractions generated from cells treated with 10µM or 40 µM H_2O_2 confirms increased H_2O_2-induced nuclear localisation of AIF in ATM-null CLL. (G) The AIF-inhibitor, N-phenylmaleimide (50µM AIFi) reduced the generation of ~50kb DNA fragments in H_2O_2-treated primary CLL tumours. Agarose plugs containing cells treated as indicated were subjected to pulsed field gel electrophoresis as described (50) and the separated DNA was visualised with ethidium bromide. The statistical significance was determined using Student's *t*-test, p-values less than 0.05 (*) were considered significant. Error bars represent SEM.

A

B

C

A

Surviving fraction (%)

◆ Vehicle
▲ Z-VAD-fmk

120
100
80
60
40
20
0

0   50   100   150
NAPQI (μM)

B

Surviving fraction (%)

◆ Vehicle
■ Z-VAD fmk

120
100
80
60
40
20
0

0   10   20   30   40   50
H₂O₂ μM

C

*GFP*shRNA:	+	+	-	-	+
*ATM*shRNA:	-	-	+	+	+
150μM NAPQI:	-	+	-	+	-
20mM NAC:	-	-	-	+	-
5Gy IR:	-	-	-	-	+

ATM ← 260kDa
PARP1 ← 140kDa
Cl. PARP1 ← 100kDa
β-ACTIN ← 40kDa

D

AIF   Mitotracker   DAPI

E

DAPI   AIF

Untreated

H₂O₂

Cells with nuclear AIF (%)

100
80
60
40
20
0

ATM-wt (n=2)   ATM-null (n=2)

*

F

ATM-null   ATM-wt

H₂O₂ (μM): 0 10 40   0 10 40

tAIF ← 40kDa
LAMIN B ← 70kDa

G

2kb DNA ladder | DMSO | AIFi | H₂O₂ | AIFi/H₂O₂

50kb ►
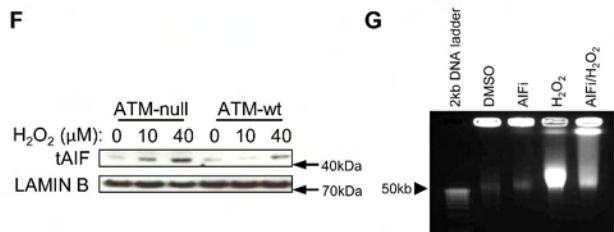
Supplementary Table S1. Characteristics of CLL samples

CLL samples were stratified based on *ATM* mutation, *TP53* mutation and 11q deletion status and phosphorylation of the ATM targets ATM, SMC1, p53 and KAP1 in response to 5Gy IR. CLL samples were considered to be *ATM* wild type (ATM-wt) if no mutation changes were detected by Sanger sequencing and if they exhibited a normal ATM-dependent response to IR. Samples were considered to be *ATM* mutant if they were found to harbour at least one mutant *ATM* allele and exhibit impaired ATM-dependent responses to DNA damage. Most *ATM* mutant tumours had evidence of biallelic *ATM* inactivation (caused by 11q deletion and an *ATM* mutation), apart from CLL69, where a single mutation rendered the ATM response to be defective.

CLL sample	TP53 mutation status	ATM mutation status	11q deletion	Biallelic or monoallelic ATM inactivation	ATM dependent DNA damage response
CLL69	WT	6815delA	A	M	D
CLL124	WT	5228C/T	P	B	D
CLLRW	WT	2282delCT, 7890delA	A	B	D
CLL57	WT	2308G/T	P	B	D
CLLJF	WT	del49 TTCT	A	NK	D
CLL152	WT	8839A/T	P	B	D
CLL166	WT	8977C/T	P	B	D
CLL15	WT	7047C/G	P	B	D
CLL77	WT	1058del2, 5224G/C	A	B	D
CLL96	WT	5041A/G,5044G/T, ins9(exon 22)	A	B	D
CLLCW	WT	WT	A	A	NK
CLLHR	WT	WT	A	A	N
CLL158	WT	WT	A	A	N
CLLRR	WT	WT	A	A	N
CLLJW	WT	WT	A	A	N
CLL17	WT	WT	A	A	N
CLL133	WT	WT	A	A	N
CLL23	WT	WT	A	A	N
CLLLP	WT	WT	A	A	NK
CLLJB	WT	WT	A	A	N
CLLVM	WT	WT	A	A	N
CLLAC	WT	WT	A	A	N
CLLMM	WT	WT	P	M	NK
CLLBK	WT	WT	P	M	NK
CLL172	WT	WT	P	M	NK
CLL48	658del2, 849insC	WT	A	A	NK
CLL120	752T/G, 830del21	WT	A	A	N
CLL117	711G/A	WT	A	A	N

Key: P=present; A=absent; NK=not known; WT= wild type; M=monoallelic; B=biallelic; D=defective; N=normal

Supplementary Table S2. Comparison of PTL yield from different plant source extractions

Entry	Plant type	Fresh plant matter (kg)	Crude extract (g)	Parthenolide (g)	w/w % content
1	Feverfew source 1 (*Tanacetum parthenium*)[a]	4.57	19.259	1.319	0.029
2	Golden Dwarf Feverfew (*Tanacetum parthenium aureum*)[a]	0.076	0.213	0.061	0.080
3	Feverfew source 2 (*Tanacetum parthenium*)[b]	1.91	7.740	1.076	0.056
4	Feverfew source 3 (*Tanacetum parthenium*)[c]	5.27	21.270	1.846	0.035
5	Tansy (*Tanacetum vulgare*)[a]	5.70	14.491	4.865	0.085

[a]Seeds purchased from *CN Seeds* and grown under glass at Winterbourne Botanic Garden (Birmingham, UK)

[b]Seed heads collect from plants in the Birmingham local area and grown under glass at Winterbourne Botanic Garden (Birmingham, UK)

[c]Self sown plants collect from the grounds of Winterbourne Botanic Garden (Birmingham, UK) and maintained under glass.

Supplementary Table S3. Primer sequences for Q-PCR

Gene	Forward	Reverse
NRF2	CGGTATGCAACAGGACATTG	GTTTGGCTTCTGGACTTGGA
NQO1	GCCGCAGACCTTGTGATATT	TGAACACTCGCTCAAACCAG
GCLM	CCAGATGTCTTGGAATGCAC	CCATGTCAACTGCACTTCT
GSR	ACTTGCCCATCGACTTTTTG	CATCTTCCGTGAGTCCCACT
HMOX1	CCAGGCAGAGAATGCTGAGT	CTTGTTGCGCTCAATCTCCT
β-ACTIN	CACCATTGGCAATGAGCGGTTC	AGGTCTTTGCGGATGTCCACGT

Supplementary Table S4. SiRNAs sequences for transient transfection.

Gene	Forward	Reverse
ATM	Stealth siRNA (Life Technologies)	Stealth siRNA (Life Technologies)
KEAP1	GGCCUUUUGGCAUCAUGAAC[dT][dT]	GUUCAUGAUGCCAAAGGCC[dT][dT]
BRCA1-1	GCUCCUCUCACUCUUCAGU[dT][dT]	ACUGAAGAGUGAGAGGAGC[dT][dT]
BRCA1-2	AAGCUCCUCUCACUCUUCAGC[dT][dT]	ACUGAAGAGUGAGAGGAGCUU[dT][dT]
Scrambled	UGUGCACGUGCCGCUCGUC[dT][dT]	GACGAGCGGCACGUGCACA[dT][dT]

Supplementary materials and methods

Extraction and derivatisation of parthenolide

General Information

Commercially available solvents and reagents were used without further purification. ^{1}H NMR spectra were recorded at 400 MHz on a Bruker AVIII400 NMR spectrometer at room temperature. ^{13}C NMR spectra were recorded at 101 MHz on a Bruker AVIII400 NMR spectrometer at room temperature and are proton decoupled. All 2D NMR spectra were recorded on a Bruker AVIII400 NMR spectrometer at room temperature. Data was processed on Mestrec version 6.0.2-5475 and Topspin 2.0 (version of Nov 9th 2006). Chemical shifts (δ) are reported in ppm relative to residual NMR solvent peaks for ^{1}H NMR and ^{13}C NMR, coupling constants (*J*) are expressed in Hertz (Hz). Mass spectra were recorded with an electrospray MS Waters LCT time of flight Mass spectrometer or with an EI (GC/MS) Waters GCT Premier Time of Flight Mass Spectrometer. Infrared spectra were recorded on a PerkinElmer 100FT-IR spectrometer at room temperature.

Extraction

(3a*S*,9a*R*,10a*R*,10b*S*,*E*)-6,9a-Dimethyl-3-methylene-3a,4,5,8,9,9a,10a,10b-octahydrooxireno[2',3':9,10]cyclodeca[1,2-b]furan-2(3H)-one (PTL)

Fresh plant matter (detailed in Supplementary Table S2) was chopped into small pieces and manually stirred in water (80 °C, 200 gL^{-1}) for 10 minutes. The resulting solution was filtered and the filtrate extracted with chloroform (2:1 aqueous:organic). The organic phases were combined, dried over MgSO$_4$ and reduced *in vacuo* to afford a brown viscous oil. This was purified by column chromatography on a CombiFlash R$_F$ 200i with a 330g silica column cartridge, ELSD detection using an ethyl acetate/hexane gradient method to afford crude parthenolide as a yellow solid. Recrystallisation from hexane/ethyl acetate afforded parthenolide as a colourless crystalline solid. Absolute stereochemistry was confirmed by X-ray crystallography. Crystal data: C$_{15}$H$_{20}$O$_3$, *M*= 248.31, orthorhombic, *a*= 11.80140(10), *b*= 11.97233(9), *c*= 18.82978(13) Å, *U*= 2660.46(3) Å^3, *T*= 99.99(10) K, space group $P2_12_12_1$, *Z*= 8 and *Z'*= 2, 25179 reflections measured, 5341 unique (*R*int= 0.0225) which were used in all calculations. The final *R*1 was 0.0268 (*I*>2σ(*I*)) and w*R*(F2) was 0.0693 (all data). Flack parameter = 0.01(4). This structure is a polymorph of an X-ray crystal structure determined at room temperature with *Z'*= 1 published on three previous occasions; CSD ref codes: ARTINB, ARTINB01 and ARTINB02.[1] CCDC-1012153 contains the supplementary crystallographic data for this structure. These data can be obtained free of charge from The Cambridge Crystallographic Data Centre *via* http://www.ccdc.cam.ac.uk/Community/Requestastructure/pages/DataRequest.aspx.

^{1}H NMR (400 MHz, CDCl$_3$): δ (ppm) 6.33 (d, *J* = 3.7, 1H), 5.63 (d, *J* = 3.3, 1H), 5.21 (dd, *J* = 12.1, 2.5, 1H), 3.86 (t, *J* = 8.6, 1H), 2.85 – 2.72 (m, 2H), 2.51 – 2.32 (m, 2H), 2.24 – 2.07 (m, 4H), 1.79 – 1.68 (m, 4H), 1.33 – 1.20 (m, 4H).; ^{13}C NMR (101 MHz, CDCl$_3$): δ (ppm) 169.3, 139.3, 134.6, 125.3, 121.2, 82.5, 66.4, 61.5, 47.7, 41.2, 36.4, 30.7, 24.2, 17.3, 17.0.; FT-IR (ATR): v (cm^{-1}) 1656.46, 1752.65, 2862.90, 2933.53, 2980.48.;MS (TOF ES+): (m/z) 249.1 [M+H]$^+$, 271.1 [M+Na]$^+$, 287.1 [M+K]$^+$.; HRMS (m/z): [M]$^+$ Calcd for C$_{15}$H$_{20}$NaO$_3$, 271.1310; found, 271.1311.; mp: 114-116 °C (Supplementary Figures S1A and S1B).

Synthesis

(3*R*,3a*S*,9a*R*,10a*R*,10b*S*,*E*)-3-((Dimethylamino)methyl)-6,9a-dimethyl-3a,4,5,8,9,9a,10a,10b-octahydrooxireno[2',3':9,10]cyclodeca[1,2-b]furan-2(3H)-one (DMAPT) Dimethylamine (2M in MeOH, 1.2 mL, 2.4 mmol, 1.5 equiv.) was added to a stirred solution of parthenolide (400 mg, 1.6 mmol, 1 equiv.) in MeOH (14 mL) for 21 hours at room temperature (Supplementary Figure S2A). The reaction mixture was reduced *in vacuo* to afford the desired compound with no further purification needed as a white solid (0.35 g, 74%). ^{1}H NMR (400 MHz, CDCl$_3$): δ (ppm) 5.21 (dd, *J* = 11.9, 2.2, 1H), 3.83 (t, *J* = 9.0, 1H), 2.78 – 2.70 (m, 2H), 2.63 (dd, *J* = 13.2, 4.8,1H), 2.47 – 2.32 (m, 2H), 2.28 – 2.01 (m, 12H), 1.70 (s, 2H), 1.69 – 1.59 (m, 1H), 1.30 (s, 3H), 1.22 (td, *J* = 13.0, 5.9, 1H).; ^{13}C NMR (101 MHz, CDCl$_3$): δ (ppm) 176.5, 134.7, 125.0, 82.1, 66.5, 61.5, 57.7, 47.9, 46.5, 46.2, 41.1, 36.7, 29.9, 24.1, 17.2, 16.9.; FT-IR (ATR): v (cm^{-1}) 1754, 2765, 2806, 2826, 2860, 2926.; MS (TOF ES+): (m/z) 294.2 [M+H]$^+$.; HRMS (m/z): [M]$^+$ Calcd for C$_{17}$H$_{28}$NO$_3$, 294.2069; found, 294.2064.; mp: 145-147 °C (Supplementary Figure S2B and S2C).

1-((3*R*,3a*S*,9a*R*,10a*R*,10b*S*,*E*)-6,9a-Dimethyl-2-oxo-2,3,3a,4,5,8,9,9a,10a,10b-decahydrooxireno[2',3':9,10]cyclodeca[1,2-b]furan-3-yl)-*N*,*N*-dimethylmethanaminium chloride (DMAPT-HCl) Hydrochloric acid gas was passed over a stirred solution of dimethylamineparthenolide (248 mg, 0.85 mmol) in Et$_2$O (50 mL) until a white precipitate formed (< 5min) (Supplementary Figure S1). The reaction mixture was reduced *in vacuo* to afford the desired compound as a white solid (0.28 g, >99%, 10:1 HCl salt:free amine by 1H NMR spectroscopy in D$_4$-MeOH). ^{1}H NMR (400 MHz, d$_4$-MeOH): δ (ppm) 5.29 (app d, *J* = 10.7, 1H), 4.17 (t, *J* = 9.1, 1H), 3.55 – 3.25 (m, 2H (minus overlapping residual MeOH CH$_3$)), 3.13 – 3.01 (m, 1H), 3.00 – 2.76 (m, 7H), 2.49 (ddd, *J* = 17.9, 13.3, 5.3 Hz, 1H), 2.36 – 1.70 (m, 10H), 1.41 – 1.10 (m, 5H).; ^{13}C NMR (101 MHz, d$_4$-MeOH): δ (ppm) 176.49, 134.46, 124.80, 83.10, 65.95, 61.91, 56.14, 47.51, 43.52, 43.15, 40.38, 36.18, 28.69, 23.58, 16.10, 15.63.; FT-IR (ATR): v (cm^{-1}) 1755, 2765, 2826, 2861, 2926, 3373 (broad).; MS (TOF ES+): (m/z) 294.2 [M+H]$^+$.; HRMS (m/z): [M]$^+$ Calcd for C$_{17}$H$_{28}$NO$_3$, 294.2069; found, 294.2066.; mp: 110-112 °C (Supplementary Figures S3A and S3B).

Cross-linking Chromatin Immunoprecipitation (XChIP)

XChIP was applied to 10-20x10^6 primary CLL cells with and without treatment with 100µM tBHQ for 6 hours. Following treatment, cells were harvested, washed three times in PBS/1µM PMSF (Sigma) and fixed in 2mM disuccinimidyl glutarate (Sigma). Cells were then fixed in 1% formaldehyde (Sigma) and cross-linking was terminated by incubation in 0.116M glycine (Sigma). To generate lysates for immunoprecipitation samples were incubated sequentially in Cell Lysis Buffer (5mM PIPES pH 8 (Sigma), 85mM KCl (Sigma), 0.5% NP40 (Sigma), 1µM PMSF, Protease inhibitor cocktail (Roche)) and RIPA Buffer (150mM NaCl (Sigma), 1% NP40, 0.5% NaDoc (Sigma), 0.1% SDS (Sigma), 50mM TrisHCl pH 8 (Sigma), 1µM PMSF, Protease inhibitor cocktail for 10 minutes followed by sonication in a Sonomatic waterbath (Model S0375) for 1 hour. Lysates were pre-cleared with Protein A sepharose beads (Sigma) and incubated overnight with 5µg of antibody or pre-immune serum. Antibody-protein/DNA complexes were immobilised on Protein A sepharose beads and DNA was recovered by incubation in Proteinase K (Ambion) followed by extraction in phenol/chloroform/isoamyl-alcohol. SYBR-green Real-Time PCR was used to quantify immunoprecipitated DNA. Data was expressed as percentage of input DNA using the comparative Ct method.

Mitochondrial ROS Assay

Mitochondrial superoxide was measured using MitoSox Red (Invitrogen) and flow cytometry in accordance with the manufacturer's instructions. Apoptotic cells were eliminated from analysis by labelling with Annexin V-APC (Invitrogen). MitoSox Red in non-apoptotic cells was quantified using a BD Biosciences LSR II flow cytometer with BD FACSDiva software. For positive and negative controls, cells were pretreated with 50µg/ml Antimycin A (Sigma) or 5µM iron (III) 5, 10, 15, 20-tetrakis-4-carboxyphenyl porphyrin (FeTCPP; Frontier Scientific Inc), respectively.

Immunoblotting

Antibodies used for immunoblotting: mouse anti-ATM , rabbit anti–phospho-ATM (Rockland Immunochemicals, PA, USA), rabbit anti-SMC1, rabbit anti-phospho SMC, rabbit anti-KAP1, rabbit anti-phospho KAP1 (Bethyl Laboratories, TX, USA), rabbit anti-phospho p53, rabbit anti-PARP (Cell Signaling, MA 01923, USA), rabbit anti-NRF2 (C20, H300), goat anti-KEAP1, rabbit anti-MafF/G/K, goat anti-BACH1, goat anti-LAM B and rabbit anti-AIF (Santa Cruz Biotechnology, Germany), rabbit anti-TUBB1 and mouse anti-β-ACTIN (Sigma-Aldrich).
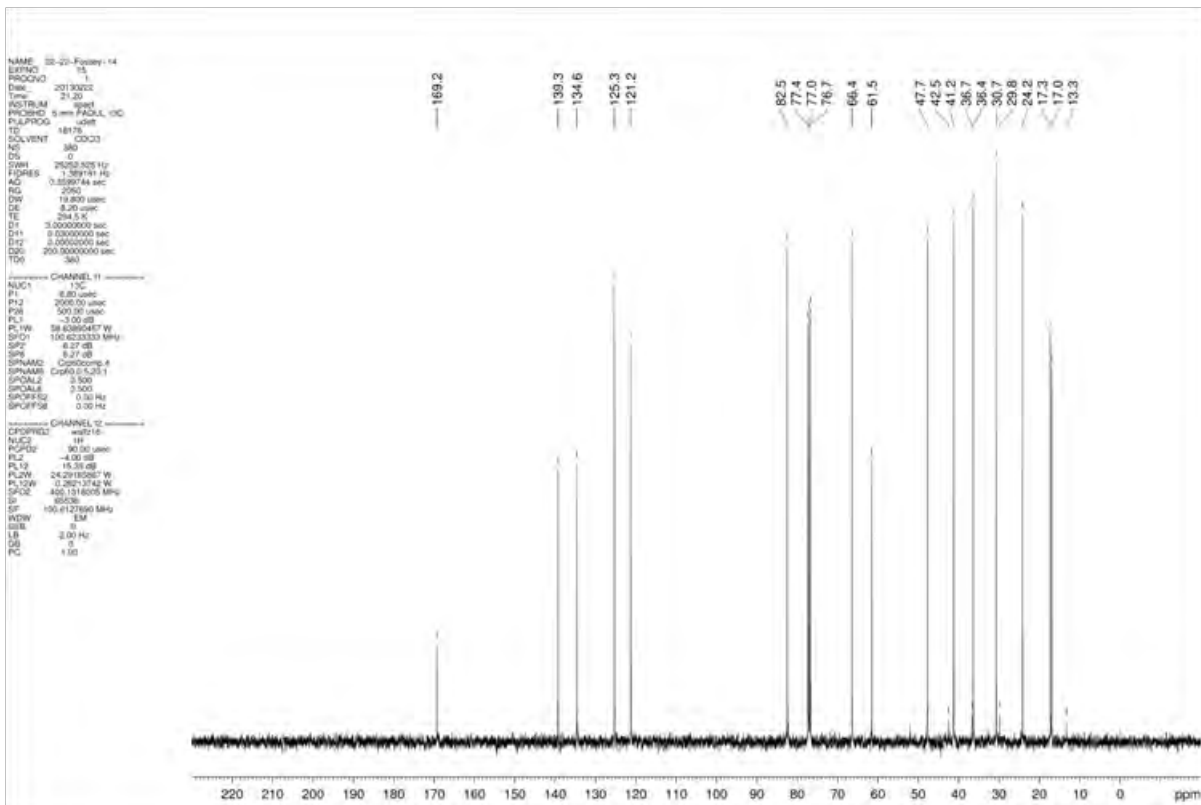
Reference

1. D.G.Leppard, M.Rey, A.S.Dreiding and R.Grieb, *Helv. Chim. Acta*, 1974, **57**, 602: M.R.Uskokovic, T.H.Williams and J.F.Blount, *Helv. Chim. Acta*, 1974, **57**, 600: I.M.Yusupova, B.Tashkhodzhaev and A.Mallabaev, *Khim.Prir.Soedin*, 1986, 788.

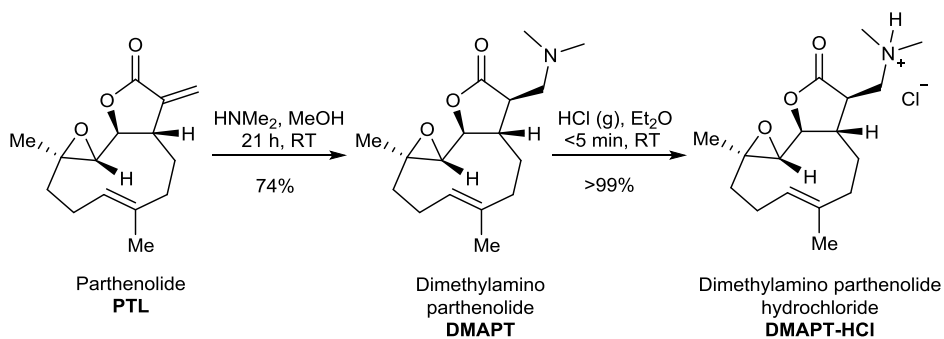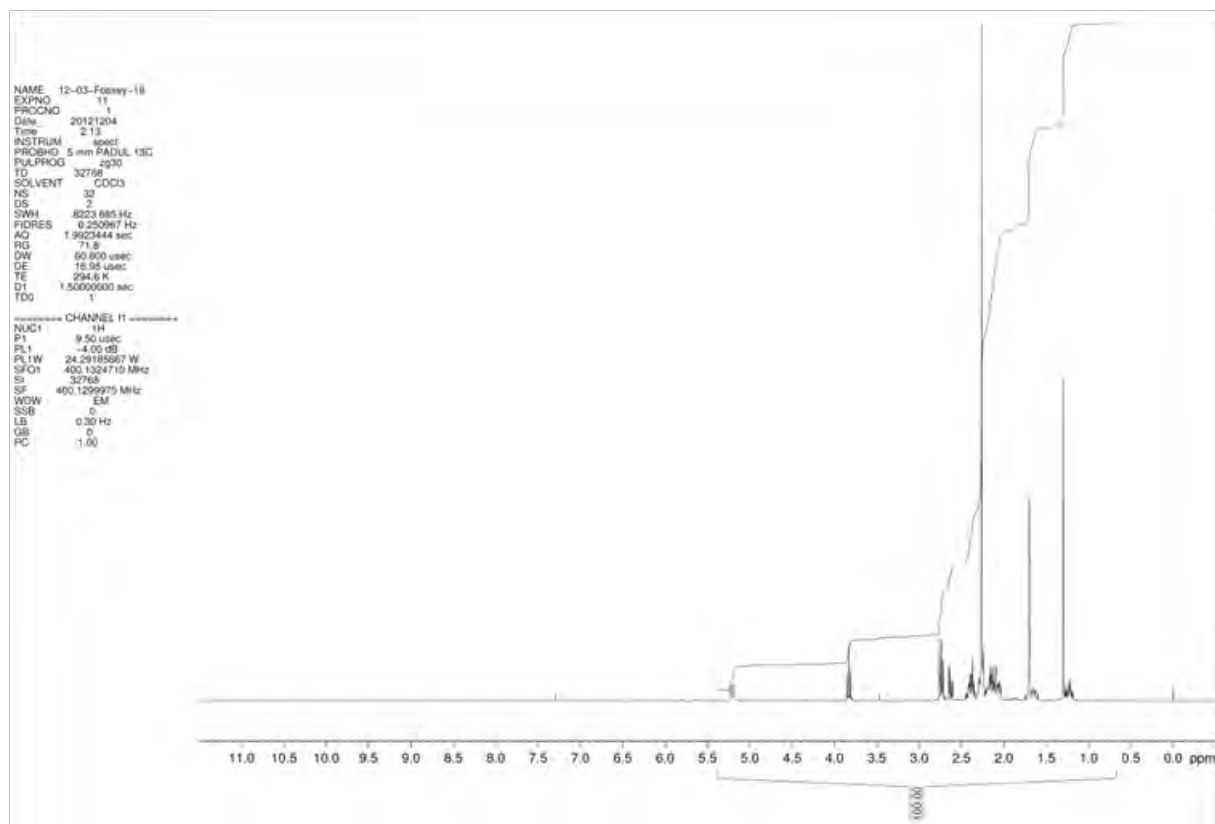**Supplementary Figure S1.** (A) ^{1}H NMR spectrum of PTL (d$_4$-MeOH) and (B) ^{13}C NMR spectrum of PTL (d$_4$-MeOH).

A

B
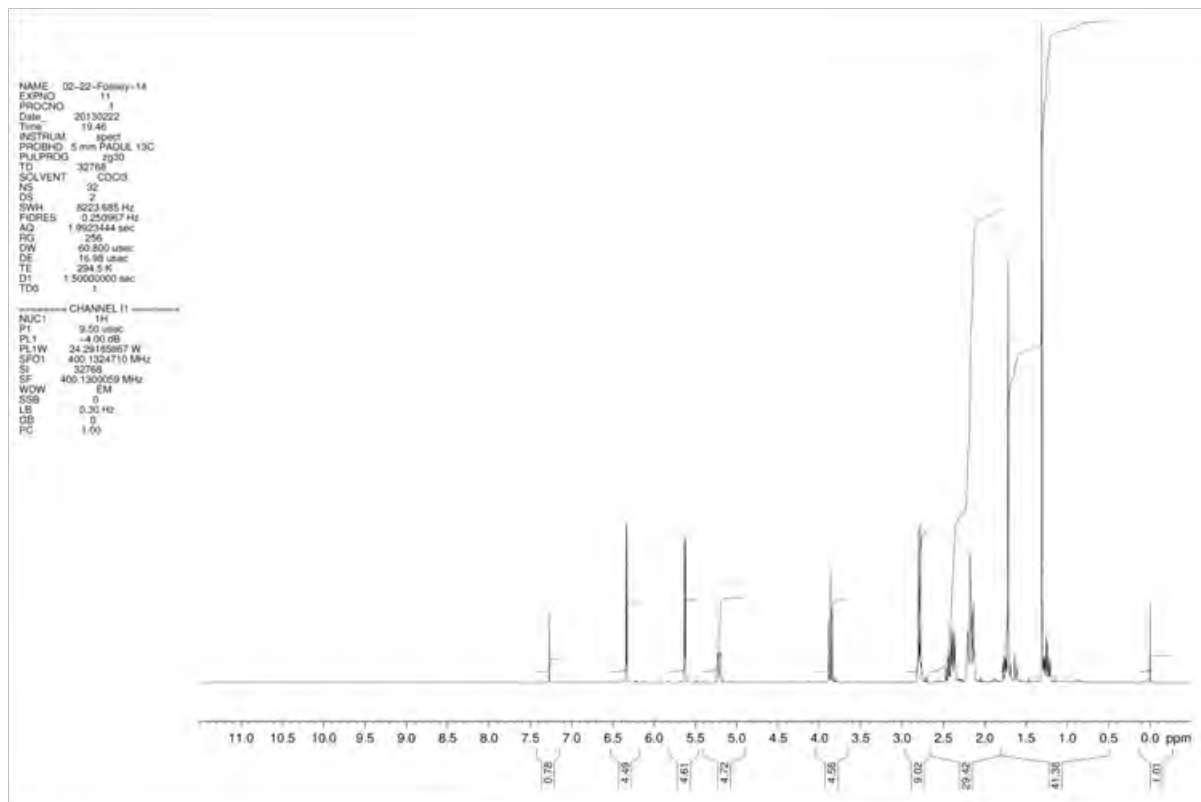
Supplementary Figure S2. (A) Schematic summarising the synthesis of DMAPT-HCl from PTL. (B) ^{1}H NMR spectrum of DMAPT (d$_4$-MeOH) and (C) ^{13}C NMR spectrum of DMAPT (d$_4$-MeOH)

A

Parthenolide	Dimethylamino	Dimethylamino parthenolide
PTL	parthenolide	hydrochloride
	DMAPT	**DMAPT-HCl**

B

C
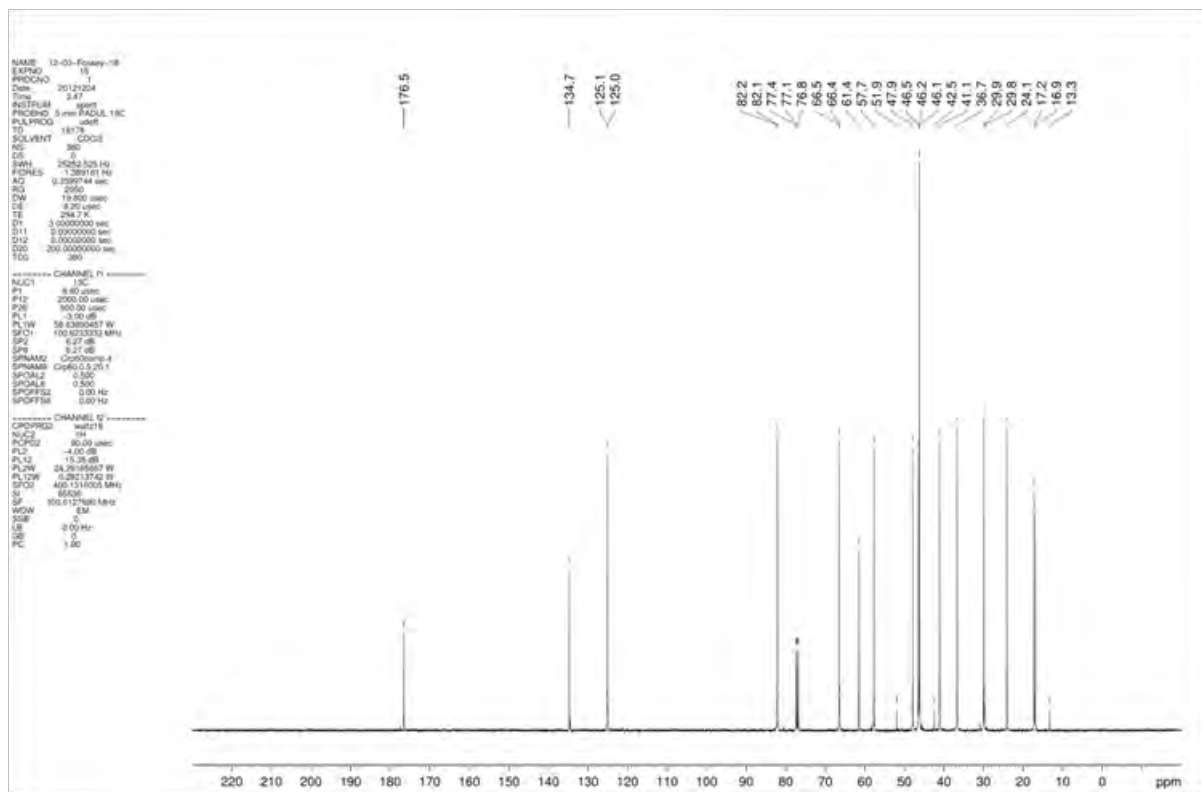
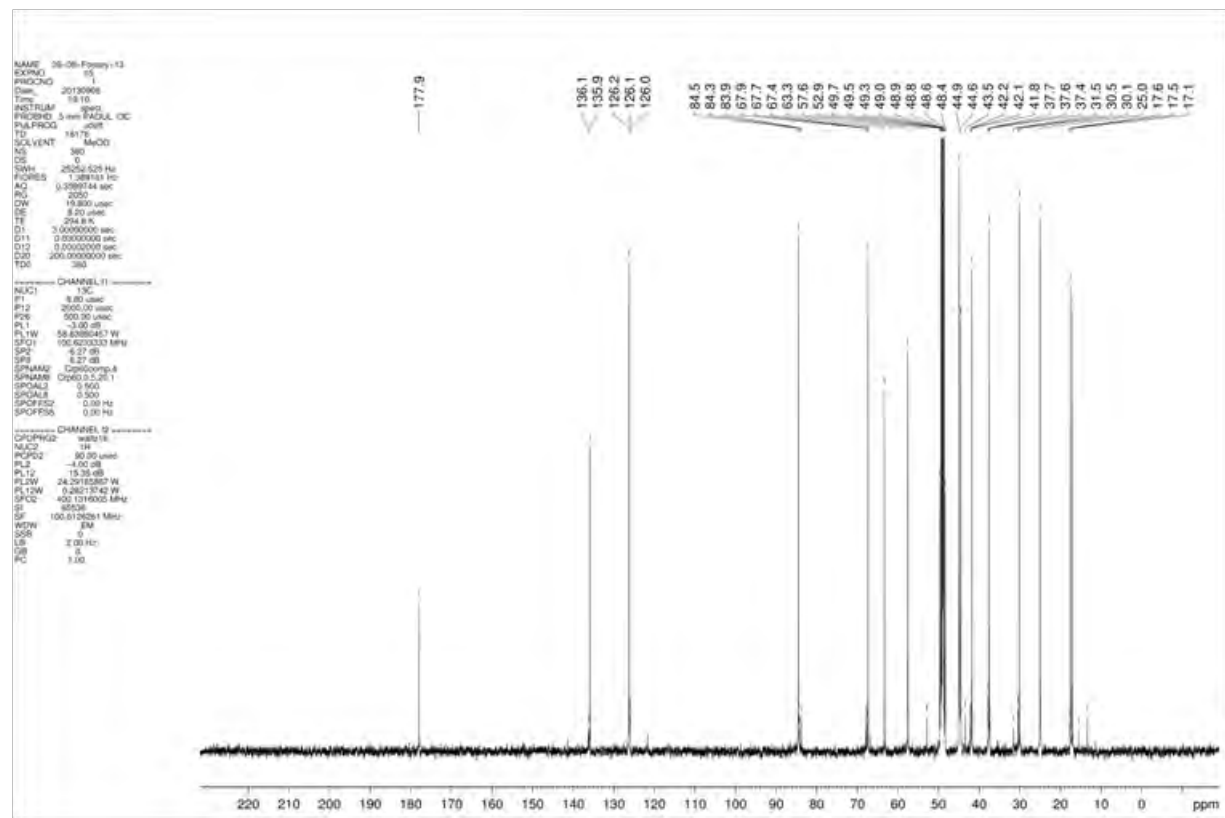**Supplementary Figure S3.** (A) ^{1}H NMR spectrum of DMAPT-HCl (d$_4$-MeOH) and (B) ^{13}C NMR spectrum of DMAPT (d$_4$-MeOH).

A


B
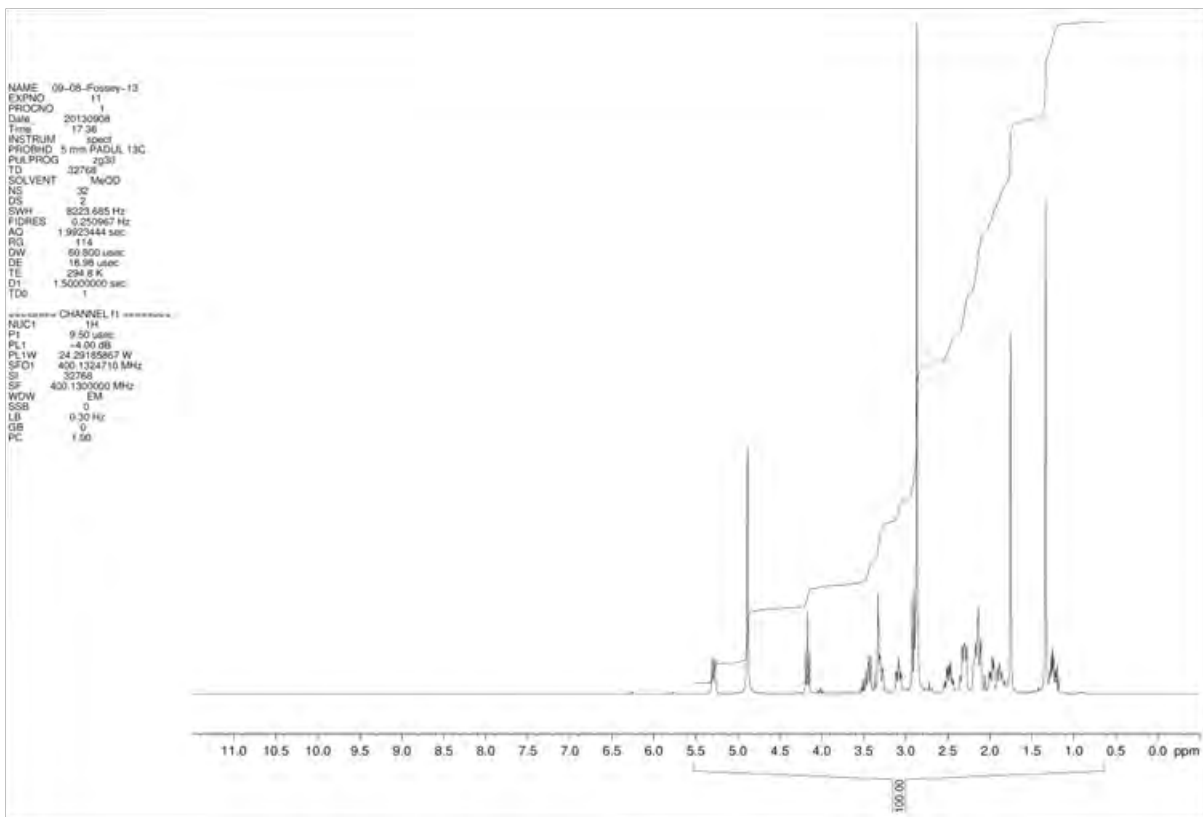
Supplementary Figure S4

(A) Heatmap of previously published microarray data (22) showing the effect of ATM-null status on the expression of 40 NRF2-target genes in response to IR. The data is normalised to the expression values in untreated cells. Each column represents a different patients sample and each row represents a single gene. Colour changes within a row indicate expression levels relative to the average of the same population. Red indicates up-regulation and blue down-regulation. (B) Q-PCR showing defective induction of NRF2-target genes in ATM-wt and ATM-null primary CLLs tumour cells following 6 hours treatment with 10μM tBHQ. (C) Dot plot comparing the ACTIN-normalised Ct values for NRF2 transcripts in ATM-wt and ATM-null primary CLL cells. (D) Immunoblot and (E) densitometric quantification showing comparable induction of NRF2 in whole cell lysates following treatment with tBHQ in a panel of ATM-wt and ATM-null primary CLL tumours. The NRF2 signal was normalised to β-ACTIN. (F) Nuclear [N] and cytoplasmic [C] fractions were generated using primary CLL samples, DMSO treated or treated with 100μM tBHQ for 6 hours. Lysates were separated by SDS-PAGE and immobilised NRF2, KEAP1, BACH1 and MAF1 were visualised using their respective antibodies (Santa Cruz). Antibodies against Lamin B and Tubulin as loading controls. The results show treatment-induced NRF2-nuclear localisation and reduction in the nuclear levels of BACH1. The levels of NRF2, KEAP1, BACH1 and MAF1 are comparable between ATM-wt and ATM-null primary CLL cells. The statistical significance was determined using Student's t-test, p-values less than 0.05 (*), 0.001 (***) were considered significant. Error bars represent SEM.
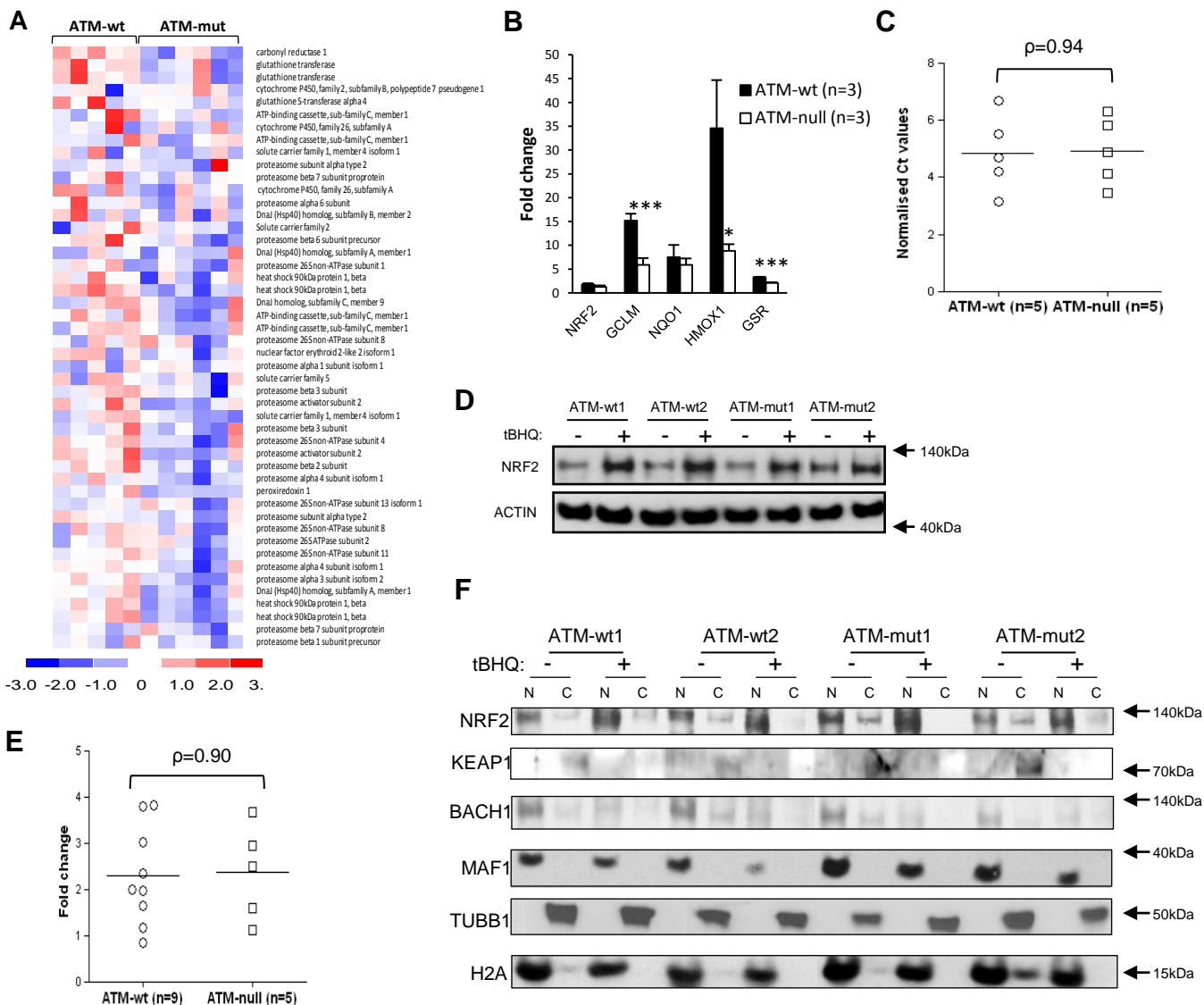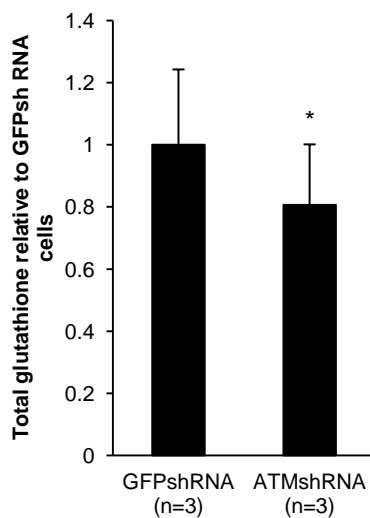
Supplementary Figure S5

A) The interaction between ATM and either NRF2 or PKCδ following treatment with IR , tBHQ or H_2O_2 was investigated in ATM-wt and A-T derived lymphoblastoid cell lines (LCLs) by co-immunoprecipitation. Cells were lysed using NETN buffer (150mM NaCl, 50mM Tris-HCl pH7.8, 1% NP40, protease inhibitor cocktail EDTA-free , 2mM $MgCl_2$ and 90U/ml Benzonase. Pre-cleared lysates containing 6mg of protein were incubated with anti-ATM (cl.11G12, Abcam) or Pre-Immune rabbit IgG (Sigma-Aldrich) and antibody-protein complexes were immobilised on Protein-A sepharose beads, separated by SDS/PAGE and subjected to immunoblotting. Neither NRF2 (rabbit anti-NRF2 (C20), Santa Cruz), or PKCδ co-immunoprecipitated with ATM in ATM-wt or ATM-null LCL cells in response to oxidative stress inducing agents (10Gy IR, 100μM tBHQ, 100μM H_2O_2). **B)** Protein lysates from CII CLL cells treated as indicated were immunoprecipitated with either anti-NRF2 (H300, Santa Cruz) or Pre-Immune IgG. Following immunoblotting of immobilised complexes the effect of ATM inhibition on the level of phospho serine in immunoprecipitated NRF2 was determined. Immunoblots were also probed for NRF2 and small MAFS. Whole cell lysates (WCL) were loaded as imput controls. **C)** Immunoblot showing comparable expression of PKCδ in ATM-wt and ATM-null primary CLLs. Antibody against SMC1 was used as a loading control.
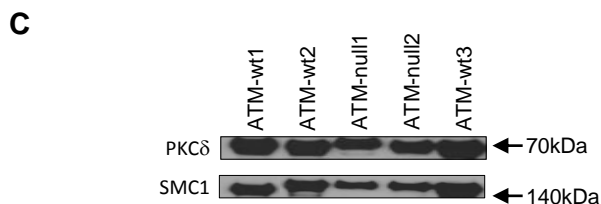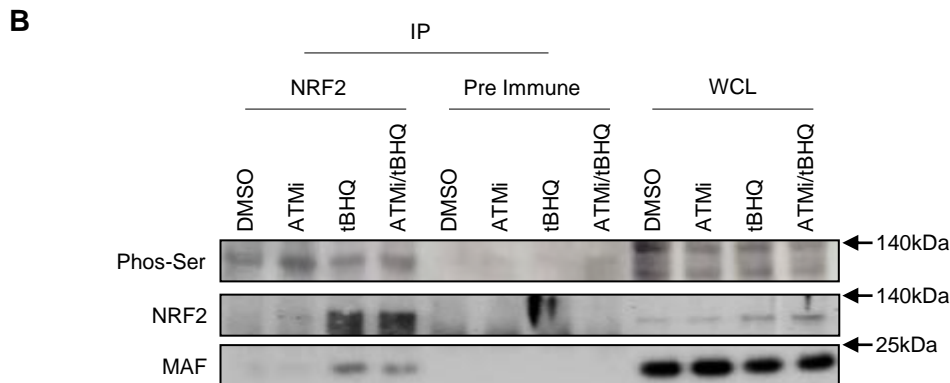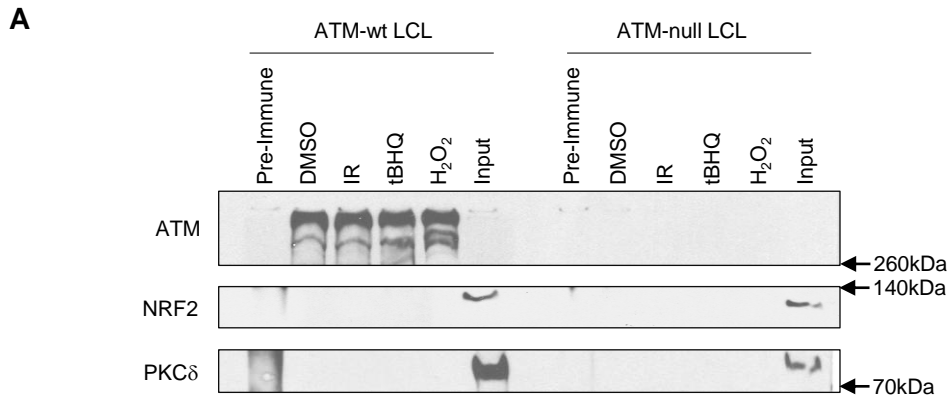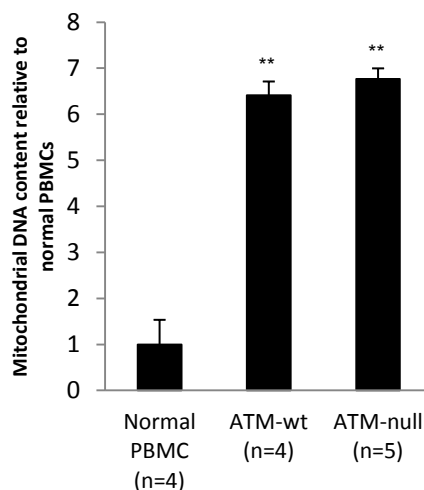
Supplementary Figure S6

(A) Total glutathione levels are reduced in three isogenic CLL cell lines (CII, PGA and HG3) with ATM knock down compared to ATM-wt counterparts. Data is expressed relative to the levels in ATM wild-type cells (GFP shRNA). (B) Q-PCR shows that the mitochondrial DNA content of both ATM-wt and ATM-null primary CLL PBMCs is increased relative to normal donor PBMCs. Mitochondrial DNA was amplified (mtFw- CACCCAAGAACAGGGTTTGT and mtRv- TGGCCATGGGTATGTTGTTAA) and normalised to genomic DNA with primers for 18S rRNA (18SFw- TAGAGGGACAAGTGGCGTTC and 18SRv- CGCTGAGCCAGTCAGTGT) using the comparative Ct method. The statistical significance was determined using Student's *t*-test, p-values less than 0.05 (*), 0.01 (**) were considered significant. Error bars represent SEM.

A

B

Supplementary Figure S7

CII isogenic cell lines exhibit increased sensitivity to (A) H_2O_2 when ATM is knocked-down. Cells stably expressing the indicated shRNAs were treated with increasing concentrations of H_2O_2 for 24 hours. (B) The sensitivity of ATM-null CLL cells to H_2O_2, (C) NAPQI or (D) parthenolide was diminished by pre-treatment with 20mM NAC. (E) PBMCs (n=2) from normal donors were treated for 24 hours with H_2O_2 or (F) parthenolide. The sensitivity of CLLs with del 11q and TP53 mutations to H_2O_2 (G) and parthenolide (H) was also examined. Surviving fraction was determined by flow cytometry following staining with Annexin V-FITC and propidium iodide. The statistical significance was determined using Student's t-test, p-values less than 0.05 (*), 0.01 (**), 0.001 (***) were considered significant. Error bars represent SEM.

Supplementary Figure S8

Immunoblot showing the effect of H_2O_2 upon phosphorylation of ATM substrates in the DNA damage response (DDR) in representative ATM-wt and ATM-null primary CLL samples. CLL samples were treated for 6 hours with the indicated concentrations of H_2O_2. For the positive control (right, last lane), protein lysate was generated from an ATM-wt sample an hour after treatment with 5 Gy ionising radiation (IR). Data shows that unlike the response to IR, ATM substrates (ATM, SMC1, KAP1 and p53) are not phosphorylated upon exposure to H_2O_2, indicating that DDR is not activated.